

AD-A098 885      NAVAL RESEARCH LAB WASHINGTON DC      F/G 20/5  
LINEAR AND NONLINEAR ELECTRON CYCLOTRON INTERACTION IN OPEN RES--ETC(U)  
MAY 81 J L VOMVORIDIS, P SPRANGLE

UNCLASSIFIED

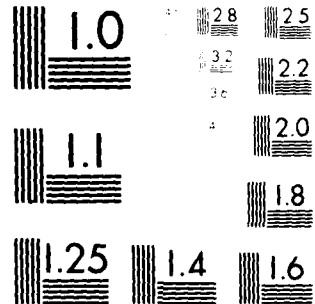
NRL-MR-4459

NL

100-1  
AFIA  
Casper

000

END  
DATE FILMED  
6-81  
DTIC



MICROGRUY RESOLUTION TEST CHART  
© 1970 AGFA-Gevaert N.V., Belgium

# Linear and Nonlinear Electron Cyclotron Interaction in Open Resonators

AD A098885

J. L. VOMVORIDIS

JAYCOR  
*Alexandria, VA 22304*

and

P. SPRANGLE

*Plasma Theory Branch  
Plasma Physics Division*

May 7, 1981



NAVAL RESEARCH LABORATORY  
Washington, D.C.

*CHMellish 11-19-81*

SECURITY CLASSIFICATION OF THIS PAGE (When Data Entered)

REPORT DOCUMENTATION PAGE		READ INSTRUCTIONS BEFORE COMPLETING FORM
1. REPORT NUMBER NRL Memorandum Report 4459	2. GOVT ACCESSION NO. <i>AD-A098 885</i>	3. RECIPIENT'S CATALOG NUMBER
4. TITLE (and Subtitle) <i>6 LINEAR AND NONLINEAR ELECTRON CYCLOTRON INTERACTION IN OPEN RESONATORS.</i>		5. TYPE OF REPORT & PERIOD COVERED Interim report on a continuing NRL problem.
7. AUTHOR(s) <i>J. L. Nomoridis* and P. Sprangle</i>	8. CONTRACT OR GRANT NUMBER(s) <i>11 711/24 121</i>	9. PERFORMING ORGANIZATION NAME AND ADDRESS Naval Research Laboratory Washington, DC 20375
10. PERFORMING ORGANIZATION NAME AND ADDRESS Department of Energy Washington, DC 20545	11. PROGRAM ELEMENT, PROJECT, TASK AREA & WORK UNIT NUMBERS 47-0865-0-1	12. REPORT DATE May 7, 1981
13. NUMBER OF PAGES 56	14. MONITORING AGENCY NAME & ADDRESS (if different from Controlling Office)	15. SECURITY CLASS. (of this report) UNCLASSIFIED
16. DISTRIBUTION STATEMENT (of this Report)  Approved for public release; distribution unlimited.	17. DISTRIBUTION STATEMENT (of the abstract entered in Block 20, if different from Report)	18. SUPPLEMENTARY NOTES  *Present address: JAYCOR, Alexandria, VA 22304
19. KEY WORDS (Continue on reverse side if necessary and identify by block number) Relativistic electron-cyclotron-maser Electron cyclotron beam Plane wave radiation Beam-wave interaction	20. ABSTRACT (Continue on reverse side if necessary and identify by block number) <p>In this work the electron cyclotron maser oscillator interaction is analyzed in an open resonator configuration. One of the salient features of this configuration for generating high power short wavelength radiation is its ability to mode select. Both the linear and nonlinear analysis are developed for an arbitrary value of the refractive index <math>n = kc/\omega</math>. Specializing to luminous waves, <math>n \rightarrow 1</math>, it is shown that the linear gain curve is symmetric</p> <p style="text-align: right;">(Continues) <i>as n &gt; 1</i></p>	Open resonator

DD FORM 1 JAN 73 1473 EDITION OF 1 NOV 65 IS OBSOLETE  
S/N 0102-014-6601

SECURITY CLASSIFICATION OF THIS PAGE (When Data Entered)

*131159*

20. ABSTRACT (Continued)

about synchronism and that instability can occur even at exact synchronism, for appropriate initial beam distributions. The nonlinear integrals of the motion are obtained, indicating that the total energy is available, the nonlinear evolution is described by a single differential equation, and the nonlinear efficiency is shown to depend on only four combinations of the beam, field, and resonator parameters. Nonlinear efficiencies up to 15% can be achieved. For a relativistic beam, a substantial frequency upshift is possible, with efficiencies up to 10%. Efficiency enhancement is possible, e.g., by the introduction of a two-stage resonator. In such a configuration, efficiencies exceeding 30% are calculated. Finally, the requirements for beam temperature and mode selectivity are found not to be particularly restrictive.

R

## CONTENTS

I. INTRODUCTION .....	1
II. LINEAR THEORY .....	6
III. NONLINEAR THEORY .....	17
IV. DISCUSSION .....	35
ACKNOWLEDGMENTS .....	44
REFERENCES .....	45

Accession For	
NTIS GRA&I	<input checked="" type="checkbox"/>
DTIC TAB	<input type="checkbox"/>
Unannounced	<input type="checkbox"/>
Justification	
By _____	
Distribution/	
Availability Codes	
Avail and/or	
Dist	Special
A	

## LIST OF FIGURES

1. Schematic representation of the quasi-optical resonator .....	2
2. Linear efficiency vs. resonator length .....	15
3. Phase space trajectories .....	23
4. Comparison of phase space trajectories .....	25
5. Contour plots for the efficiency coefficient $C_\eta$ .....	28
6. Contour plots for the anisotropy constant $C_d$ .....	29
7. Spatial evolution of the normalized efficiency .....	31
8. Contour plots of the normalized efficiency .....	32
9. Optimal normalized efficiency .....	34
10. Efficiency enhancement in a two-stage oscillator configuration .....	42

## LINEAR AND NONLINEAR ELECTRON CYCLOTRON INTERACTION IN OPEN RESONATORS

### I. INTRODUCTION

One of the most recently developed devices for the generation of coherent radiation in the millimeter and centimeter range is the gyrotron (or, electron cyclotron maser). In this device, radiation power is produced by the interaction of the TE fields of the cavity with an electron beam which propagates and gyrates along an external static magnetic field. This interaction has been studied extensively,<sup>1-18</sup> both theoretically and experimentally, with impressive results, such as a 22% efficiency of conversion of beam kinetic power to radiation at a 2 mm wavelength with 22 kW CW output power. Substantial improvements are possible if axial nonuniformities are introduced in the form of gradients either in the oscillator cross-section,<sup>19,20</sup> or in the external magnetic field.<sup>21-23</sup>

The frequency of the gyrotron is determined by the relativistic gyrofrequency of the electrons in the external magnetic field. For efficient operation, this gyrofrequency, Doppler-shifted in the electron beam rest frame, must be in close synchronism with the eigenfrequency of the cavity. However, since the size of the cavity cannot be made arbitrarily small, a large value of the gyrofrequency may result in synchronism with more than one of the cavity eigenfrequencies. Although preliminary investigations<sup>24-28</sup> have not been conclusive, it is expected that multi-mode effects may prove a problem for wavelengths less than  $\sim 1$  mm.

To avoid such potential limitations, it is proposed that the gyrotron cavity be replaced by an open quasi-optical resonator, Fig. 1, formed by two mirrors of appropriate shape. Taking the z-axis as the axis of the radiation, the fields can be shown to be derivable from the usual vector potential

Manuscript submitted March 10, 1981.

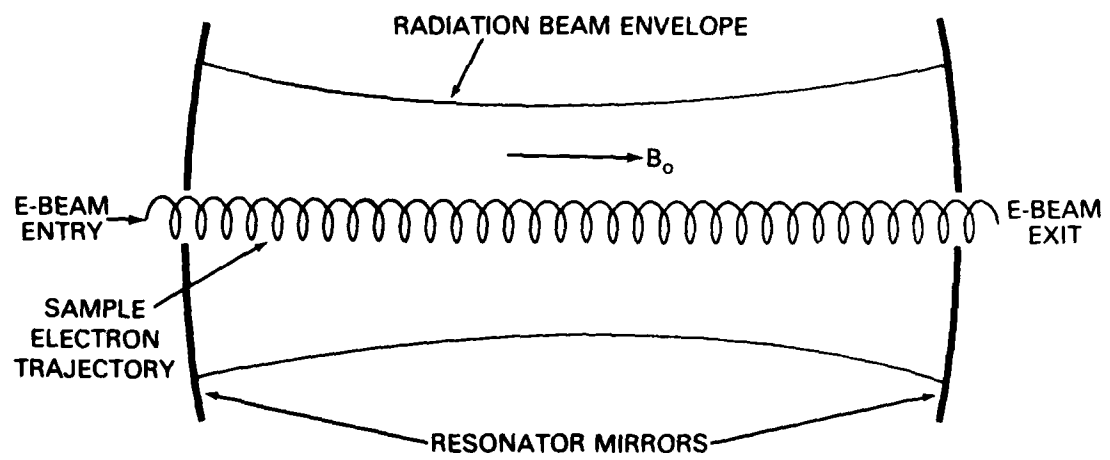


Fig. 1 — Schematic representation of the quasi-optical resonator and electron beam configuration. The diffracted fields are contained by the two mirrors, one or both of which may be partially transmitting. The individual electrons of the beam execute, to zero order, a helical motion in the external magnetic field  $B_o$ .

$$A = 2A(r,z) \sin [kz + \alpha(r,z)] [\hat{e}_x \cos(\omega t) + \epsilon \hat{e}_y \sin(\omega t)] \\ + \frac{2}{kr} \frac{\partial}{\partial r} [A \cos(kz + \alpha)] [x \cos(\omega t) + \epsilon y \sin(\omega t)] \hat{e}_z \quad (1)$$

where  $\omega$  is the radiation frequency,  $k = \omega/c$  is the dominant term of the wavenumber,  $\alpha(r,z) = kr^2/2R + \tan^{-1}(z/z_0)$  is the spatially dependent phase,  $A(r,z) = A_0(r_0/r_s) \exp(-r^2/r_s^2)$  is the position dependent amplitude for the fundamental mode,  $\epsilon$  is the ellipticity of the radiation,  $r = (x^2 + y^2)^{1/2}$  is the transverse coordinate,  $r_s(z) = r_0(1 + z^2/z_0^2)$  is the spot size at  $z$  with  $r_0$  its minimum value at  $z=0$ ,  $R(z) = z(1 + z_0^2/z^2)$  is the radius of curvature of the wave front at  $z$ ,  $z_0 = \pi r_0^2/\lambda$  is the Rayleigh length, and  $\lambda = 2\pi/k$  is the wavelength. The diffraction angle of the fundamental mode is  $\theta_d = \lambda/\pi r_0$ . The diffraction angle of the higher order modes is larger. Therefore, if the radius of the mirrors is somewhat larger than  $r_s$ , most of the energy of the fundamental mode will be intercepted, resulting in a high value of  $Q$ . The higher order modes on the other hand will suffer from diffraction losses, their  $Q$ 's will be small, and therefore these modes will not be excited. Thus the introduction of open resonators provides an effective natural means for transverse mode selection.

This paper is intended as a preliminary but comprehensive analysis of the electron cyclotron interaction with the diffracted fields of Eq. (1). The limit we have considered throughout the paper is that of an electron beam propagating along the radiation axis.<sup>29</sup> We have assumed that the transverse extent of the beam is small compared to the radiation spot size  $r_s$ , therefore the action of the field on the beam electrons is that of a plane wave. In this limit we have developed the linear theory

(Sec. II) and the nonlinear theory (Sec. III) of the interaction in a bounded system (oscillator). Various issues pertaining to the basic theory are discussed in Sec. IV, along with the presentation of numerical examples.

In Section II the linear dispersion relation is obtained for an oscillator. For the sake of generality, an arbitrary electron beam distribution is assumed. All forward and backward components of the field perturbation are kept and the value of the refractive index  $n = kc/\omega$  is left unspecified in the bulk of the analysis in this Section. Specializing to the case of a monoenergetic beam, affected only by the forward wave,<sup>30</sup> yields a compact result and reproduces the expressions for the gyrotron in the cut-off frame, when  $n \rightarrow 0$ . For luminous waves,  $n \rightarrow 1$ , the gain curve has two interesting features, viz. it possesses even symmetry about the frequency of synchronism and can lead to instability even at exact synchronism, provided that the transverse beam velocity satisfies a certain inequality.

The nonlinear theory is developed in Section III for a constant amplitude wave. The equations of motion for the electrons are expressed using the axial coordinate  $z$  as the independent Lagrangian variable. These equations are interrelated by four invariants. Two of these invariants relate the transverse displacement to the velocity, while the other two relate the velocity components. These invariants reproduce earlier results when  $n \rightarrow 0$  or  $n \rightarrow 1$ . A transformation to slowly varying variables eliminates an additional variable and results in a single integrable equation. The phase space plots are studied and distinction between closed and open orbits is made. A condition for complete electron

kinetic energy depletion is identified. The nonlinear efficiency is found to depend on only four combinations of the field and electron beam parameters and is conveniently presented in contour plots.

Finally, certain aspects related to the applicability of our analysis are discussed in Section IV. It is shown that the symmetry of the gain spectrum can be used to relax the temperature requirements. The interaction is also shown to have inherent abilities for axial mode selection. In our example of a gyrotron type operation we obtained a 13.7% efficiency at  $\lambda = 2$  mm with a 61 kW output power. The potential application of this interaction as a free-electron laser is discussed and a scheme for efficiency enhancement is proposed. By utilizing a two-oscillator configuration, an efficiency  $\eta = 35\%$  is obtained, while estimates predict efficiencies can reach 60%.

The cyclotron interaction of electrons with luminous waves has been the subject of two recent investigations.<sup>31,32</sup> In the first paper the dispersion relation was obtained and analyzed for waves with arbitrary values of  $n = kc/\omega$  in the limit of vanishing axial beam velocity. In the second paper the stability was investigated in terms of particle energy loss, obtained from an expansion of the equations of motion in the radiation field amplitude. Both these analyses assume a uniform medium of infinite extend in  $z$  and use the time as the independent coordinate. Accordingly, their results differ from ours, since in the present work the axial position  $z$  is used as the independent variable and the presence of the oscillator boundaries is important.

## II. LINEAR THEORY

The fields of the oscillator are given in terms of the vector potential  $\underline{A}$  by the simplification of Eq. (1),

$$\begin{aligned}\underline{A} &= A_0 \sin(kz) (\hat{\underline{e}}_x + i\varepsilon \hat{\underline{e}}_y) e^{-i\omega t} + c.c. \\ &= 2A_0 \sin(kz) [\hat{\underline{e}}_x \cos(\omega_R t) + \varepsilon \hat{\underline{e}}_y \sin(\omega_R t)] e^{i\Gamma t},\end{aligned}\tag{2}$$

where  $A_0$  is the amplitude,  $k$  is the axial wavenumber (along the  $z$  axis),  $\omega$  is the complex frequency consisting of the real frequency and the growth rate,  $\omega = \omega_R + i\Gamma$ ,  $\varepsilon$  characterizes the ellipticity of the polarization, and  $\hat{\underline{e}}_x$  and  $\hat{\underline{e}}_y$  are unit transverse vectors. The oscillator fields  $\delta\underline{E}$  and  $\delta\underline{B}$  are given by

$$\begin{aligned}\delta\underline{E} &= -\frac{1}{c} \frac{\partial \underline{A}}{\partial t} = i \frac{\omega}{c} A_0 \sin(kz) (\hat{\underline{e}}_x + i\varepsilon \hat{\underline{e}}_y) e^{-i\omega t} + c.c., \\ \delta\underline{B} &= \nabla \times \underline{A} = -ikA_0 \cos(kz) (\varepsilon \hat{\underline{e}}_x + i \hat{\underline{e}}_y) e^{-i\omega t} + c.c.\end{aligned}\tag{3}$$

In addition, a static uniform axial magnetic field is present,  $\underline{B}_0 = B_0 \hat{\underline{e}}_z$ .

The fields given by Eq. (3) are appropriate for those in an oscillator formed by two parallel plates of infinite extent in the transverse direction. They are also applicable to a general case of an oscillator consisting of two concave boundaries, provided that  $A_0$  and  $k$  are appropriate functions of  $x$ ,  $y$ , and  $z$  and the small axial field components are included. These modifications depend on the waist of the radiation field,  $r_0$ , and the Rayleigh length  $z_0 = \omega r_0^2/2c$  and are negligible if the beam width and

the electron Larmor radius are small compared to  $r_0$ , and if the axial interaction length is small compared to  $z_0$ . Accordingly, under such conditions the fields in Eq. (3) can be used with  $A_0$  and  $k$  constant.

The behavior of the field is governed by the wave equation,

$$-\nabla^2 \underline{A} + \frac{1}{c^2} \left( \frac{\partial^2}{\partial t^2} + v \frac{\partial}{\partial t} \right) \underline{A} = \frac{4\pi}{c} \underline{J}, \quad (4)$$

where  $v$  is a real quantity representing losses. It will be shown later that  $v = \omega_R/Q$ , where  $Q$  is the quality factor of the resonator. Expressing the current density as

$$\underline{J} = \tilde{J} e^{-i\omega t} + c.c., \quad (5)$$

it is found that Eq. (4) together with Eq. (2) can be put in the form

$$\begin{aligned} & \frac{1}{2} \left[ (k^2 c^2 - \omega_R^2) - i(2\Gamma + v)\omega_R \right] A_0 (\hat{e}_x + i\varepsilon \hat{e}_y) \\ &= \int_0^L 4\pi c \tilde{J} \sin(kz) dz, \end{aligned} \quad (6)$$

where  $L$  is the interaction length.

Before continuing, it is necessary to evaluate  $v$  in Eq. (6). This is accomplished by integrating Poynting's theorem along the interaction region,

$$\frac{\partial}{\partial t} \int_0^L u dz + S_z(z=L) - S_z(z=0) = - \int_0^L \delta \underline{E} \cdot \underline{J} dz, \quad (7)$$

where  $u$  is the radiation energy density and the  $z$  component of Poynting's vector  $S_z$  vanishes at  $z=0$  and has the value  $S_z = (\omega_R/Q) \int_0^L u dz$  at  $z=L$ , by the definition of  $Q$ . The definition of  $\Gamma$  implies an exponential variation,  $\exp(2\Gamma t)$ , for the energy, thus

$$(2\Gamma + \frac{\omega_R}{Q}) \int_0^L u dz = - \int_0^L \delta E \cdot \vec{J} dz , \quad (8)$$

and from a comparison with Eq. (6) it is seen that

$$v = \frac{\omega_R}{Q} . \quad (9)$$

The current density in Eq. (6) will be evaluated from the appropriate moment of the distribution function, the latter obtained from the solution of the Vlasov equation. Employing the expansion  $f = f^{(0)} + f^{(1)}$  of the distribution function,  $f^{(0)}$  describes the zero-order trajectories in the external magnetic field and is therefore a function of the corresponding constants of motion,

$$\begin{aligned} p_{\perp}^2 &= p_x^2 + p_y^2 , \\ \theta &= \tan^{-1} \left( \frac{p_y}{p_x} \right) - \frac{\Omega_0 m_0}{p_z} z , \\ p_{||} &= p_z , \\ x_g &= x - \frac{p_y}{\Omega_0 m_0} , \\ y_g &= y + \frac{p_x}{\Omega_0 m_0} , \end{aligned} \quad (10)$$

which are, respectively, the transverse momentum, the azimuthal phase angle relative to a fixed cyclotron helix, the parallel momentum, and the

$x$  and  $y$  locations of the guiding center, defined as functions of the Cartesian components of position ( $x, y, z$ ) and momentum ( $p_x, p_y, p_z$ ). The nonrelativistic cyclotron frequency is  $\Omega_0 = eB_0/m_0c$ . Considering Eq. (10) as a transformation from Cartesian to constant-of-motion phase space, that is, defining  $g^{(0)} = f^{(0)}$  and  $g^{(1)} = f^{(1)}$ , where  $g^{(0)}$  and  $g^{(1)}$  are functions of the variables defined in Eq. (10) as well as  $z$  and  $t$ , the Vlasov equations can be written as

$$\left( \frac{\partial}{\partial t} + \frac{p_{||}}{\gamma m_0} \frac{\partial}{\partial z} \right) g^{(1)} = e \left[ \delta \xi + \frac{1}{\gamma m_0 c} \vec{p} \times \delta \vec{B} \right] \cdot \frac{\partial}{\partial \vec{p}} g^{(0)} . \quad (11)$$

Here the unperturbed distribution function is assumed independent of  $\theta$ ,  $x_g$  and  $y_g$ . The relativistic factor  $\gamma$  is defined as  $\gamma^2 = 1 + (p_{||}^2 + p_{\perp}^2)/(m_0 c)^2$ .

Using Eqs. (3) and (10) and introducing the expansion

$$g^{(1)} = \tilde{g}^{(1)} e^{-i\omega t} + \text{c.c.} , \quad (12)$$

in Eq. (11), the first order linear homogeneous differential equation for  $\tilde{g}^{(1)}$  can be integrated, yielding

$$\begin{aligned} \tilde{g}^{(1)} &= \frac{1}{4} e A_0 \frac{\gamma m_0}{p_{||}} \exp \left[ i \frac{\gamma m_0 \omega}{p_{||}} z \right] \\ &\times \left\{ (1 + \epsilon) e^{i\theta} \left[ \frac{e^{i\xi_{1+} z} - 1}{i\xi_{1+}} D_+ - \frac{e^{i\xi_{1-} z} - 1}{i\xi_{1-}} D_- \right] \right. \\ &\left. - (1 - \epsilon) e^{-i\theta} \left[ \frac{e^{-i\xi_{2-} z} - 1}{i\xi_{2-}} D_+ - \frac{e^{-i\xi_{2+} z} - 1}{i\xi_{2+}} D_- \right] \right\} g^{(0)} . \quad (13) \end{aligned}$$

The differential operators,  $D_+$  and  $D_-$ , acting on  $g^{(0)}$ , and the relative wavenumbers,  $\xi_{1\pm}$  and  $\xi_{2\pm}$ , are

$$D_{\pm} = \frac{\omega}{c} \frac{\partial}{\partial p_{\perp}} \pm \frac{k}{\gamma m_0 c} \left( p_{\perp} \frac{\partial}{\partial p_{||}} - p_{||} \frac{\partial}{\partial p_{\perp}} \right)$$

$$\xi_{1\pm} = \pm k + \frac{(\Omega_0 - \gamma\omega)m_0}{p_{||}} \quad (14)$$

$$\xi_{2\pm} = \pm k + \frac{(\Omega_0 + \gamma\omega)m_0}{p_{||}} \quad .$$

The constant of integration in Eq. (13) is such that  $\tilde{g}^{(1)} = 0$  at  $z=0$ , corresponding to an unperturbed entering beam.

The perturbed distribution function, obtained in Eq. (13), can be used to evaluate the Fourier component of the current density,

$$\tilde{J} = - \frac{e}{m_0} \int \frac{p}{\gamma} \tilde{g}^{(1)} dp \quad . \quad (15)$$

Performing the integration over  $\theta$  in Eq. (15) gives

$$\begin{aligned} \tilde{J} = & - \frac{1}{8} e^2 A_0 n_0 \int dp_{\perp} dp_{||} \frac{p_{\perp}^2}{p_{||}} \exp \left[ i \frac{\gamma m_0 \omega}{p_{||}} z \right] \\ & \times \left\{ (\hat{e}_x + i \hat{e}_y) \exp \left[ -i \frac{\Omega_0 m_0}{p_{||}} z \right] (1 + \epsilon) \left[ \frac{e^{i\xi_{1+}z} - 1}{i\xi_{1+}} D_+ - \frac{e^{i\xi_{1-}z} - 1}{i\xi_{1-}} D_- \right] \right. \\ & \left. - (\hat{e}_x - i \hat{e}_y) \exp \left[ i \frac{\Omega_0 m_0}{p_{||}} z \right] (1 - \epsilon) \left[ \frac{e^{-i\xi_{2-}z} - 1}{i\xi_{2-}} D_+ - \frac{e^{-i\xi_{2+}z} - 1}{i\xi_{2+}} D_- \right] \right\} g_0 \quad . \end{aligned} \quad (16)$$

The beam density  $n_0$  has been extracted for convenience from the distribution function, by defining  $n_0 g_0 = 2\pi g^{(0)}$ , where  $g_0$  is normalized to  $\int dp_{\perp} \int dp_{||} p_{\perp} g_0 = 1$ . Finally, multiplying  $\tilde{J}$  by  $\sin(kz)$  and integrating over the length of interaction, yields the driving term required in Eq. (6),

$$\begin{aligned}
& \int_0^L 4\pi c \tilde{J} \sin(kz) dz \\
&= i \frac{\pi}{4} e^2 A_0 n_0 c \int dp_{\perp} dp_{||} \frac{p_{\perp}^2}{p_{||}} \\
&\times \left\{ (\hat{e}_x + i\hat{e}_y) (1 + \varepsilon) \left[ \left( \frac{e^{-i\xi_{1-}L} - 1}{i\xi_{1-}} - L - \frac{e^{-i\xi_{1+}L} - 1}{i\xi_{1+}} \right) \frac{1}{i\xi_{1+}} D_+ \right. \right. \\
&\quad \left. \left. - \left( L + \frac{e^{i\xi_{1-}L} - 1}{i\xi_{1-}} - \frac{e^{i\xi_{1+}L} - 1}{i\xi_{1+}} \right) \frac{1}{i\xi_{1-}} D_- \right] \right. \\
&\quad \left. - (\hat{e}_x - i\hat{e}_y) (1 - \varepsilon) \left[ \left( - \frac{e^{i\xi_{2+}L} - 1}{i\xi_{2+}} - L + \frac{e^{i\xi_{2-}L} - 1}{i\xi_{2-}} \right) \frac{1}{i\xi_{2+}} D_+ \right. \right. \\
&\quad \left. \left. - \left( L - \frac{e^{i\xi_{2+}L} - 1}{i\xi_{2+}} + \frac{e^{i\xi_{2-}L} - 1}{i\xi_{2-}} \right) \frac{1}{i\xi_{2+}} D_- \right] \right\} g_0 , \\
&\tag{17}
\end{aligned}$$

where the boundary condition  $\sin(kL) = 0$  has been used to eliminate terms similar to  $\exp[i(\xi_{1+} - \xi_{1-})L]$ .

Equating Eqs. (6) and (17) yields a consistency condition between  $\omega_R$ ,  $\Gamma$  and  $\varepsilon$ . This is the linear dispersion relation, which includes the positive and negative electron cyclotron interaction with both the forward and backward traveling waves. However, in general only one of these interactions is resonant, which we take throughout the remainder of this paper to be with the forward wave.<sup>30</sup> Defining

$$\begin{aligned}
\xi &= \xi_{1+} = k + \frac{(\Omega_0 - \gamma\omega)m_0}{p_{||}} , \\
\mu &= \frac{1}{2} \xi L , \\
&\tag{18}
\end{aligned}$$

one obtains from Eq. (17),

$$\int_0^L 4\pi c \tilde{J} \sin(kz) dz \\ = i \frac{\pi}{4} e^2 A_0 n_0 c \int dp_{\perp} dp_{||} \frac{p_{\perp}^2}{p_{||}} (\hat{e}_x + i \hat{e}_y) (1 + \epsilon) \left[ \frac{iL}{\xi} + \frac{e^{-i\xi L} - 1}{\xi^2} \right] D_+ g_0. \quad (19)$$

Comparing this equation with Eq. (6), it is seen immediately that consistency requires that  $\epsilon=1$ , that is, only a circular polarization is compatible with the interaction. The dispersion relation now becomes

$$(\omega_R^2 - k^2 c^2) + i\omega_R (2\Gamma + \frac{\omega_R}{Q}) \\ = \frac{1}{16} m_0 L c \omega_{bo}^2 \int dp_{\perp} dp_{||} \frac{p_{\perp}^2}{p_{||}} \left[ \frac{2\mu - \sin 2\mu}{\mu^2} + i 2 \frac{\sin^2 \mu}{\mu^2} \right] D_+ g_0, \quad (20)$$

where  $\omega_{bo}^2 = 4\pi e^2 n_0 / m_0$  and  $\mu$  is a complex quantity, defined in Eq. (18) and depending on  $\omega = \omega_R + i\Gamma$ .

In a number of interesting special cases only the real part  $\mu_R$  of  $\mu$  is of significance. These cases are: (i) the (linear) steady state,  $\Gamma = 0$ , (ii) the conditions just above threshold,  $\Gamma \rightarrow 0$ , and (iii) when the beam is sufficiently weak, so that the imaginary part of  $\mu$  is negligible. In such cases, separate equations can be obtained for the frequency and growth rate,

$$\omega_R^2 - (kc)^2 = \frac{1}{4} m_0 L c \omega_{bo}^2 \int dp_{\perp} dp_{||} \frac{p_{\perp}^2}{p_{||}} \frac{2\mu_R - \sin 2\mu_R}{(2\mu_R)^2} D_+ g_0, \\ \omega_R (2\Gamma + \frac{\omega_R}{Q}) = \frac{1}{8} m_0 L c \omega_{bo}^2 \int dp_{\perp} dp_{||} \frac{p_{\perp}^2}{p_{||}} \frac{\sin^2 \mu_R}{\mu_R^2} D_+ g_0. \quad (21)$$

Finally, for the special case of a monoenergetic beam,  $g_0 = \delta(p_{\perp} - p_{\perp 0}) \delta(p_{||} - p_{||0}) / p_{\perp 0}$ , integration over  $p_{\perp}$  and  $p_{||}$  gives

$$\left. \begin{array}{l} \frac{1-n^2}{2} \\ \frac{2\Gamma}{\omega_R} + \frac{1}{Q} \end{array} \right\} = \frac{1}{8} \left( \frac{\beta_{\perp 0}}{\beta_{||0}} \right)^2 \frac{\omega_{bo}^2}{\gamma_0} \frac{L}{\omega_R c} D_\mu \left\{ \begin{array}{l} R_n(\mu_R) \\ R_Q(\mu_R) \end{array} \right. , \quad (22)$$

where the refractive index,  $n = kc/\omega_R$ , has been introduced, the quantity  $\mu_R$  is obtained from Eq. (18) in terms of the beam quantities  $\gamma_0$  and  $p_{||0}$  and the dimensionless velocities  $\beta_{||0} = p_{||0}/\gamma_0 m_0 c$  and  $\beta_{\perp 0} = p_{\perp 0}/\gamma_0 m_0 c$  were used. The operator  $D_\mu$  and the functions  $R_n$  and  $R_Q$  are

$$D_\mu = \left[ n - 2 \frac{\beta_{||0}(1-n\beta_{||0})}{\beta_{\perp 0}^2} \right] + \left[ \frac{1-n^2}{2} \frac{\omega_R L}{c} + n\mu_R \right] \frac{d}{d\mu_R} ,$$

$$R_n(\mu) = \frac{2\mu - \sin 2\mu}{(2\mu)^2} , \quad (23)$$

$$R_Q(\mu) = \left( \frac{\sin \mu}{\mu} \right)^2 .$$

To complete the formalism we note that for the fields of Eq. (3) the total steady state field energy inside the interaction region,  $L$ , is given by  $\int_0^L u dz = (\omega_R A_0/2c)^2 L (1+n^2)/\pi$ , hence the efficiency of converting kinetic energy to radiation energy, per unit time, is

$$\eta_L = \frac{1+n^2}{2\gamma_0(\gamma_0-1)} \frac{\beta_{\perp 0}^2}{\beta_{||0}^3} \left( \frac{eA_0}{2mc^2} \right)^2 \left( \frac{\omega_R L}{c} \right)^2 D_\mu R_Q . \quad (24)$$

We have thus completed the linear analysis of the interaction. The results are represented by Eqs. (22) and (24) for a monoenergetic beam and weak (or vanishing) growth-rate, as well as the general case given by Eq. (20). Let us consider now the significance of these equations,

in the limiting cases  $n \rightarrow 0$  and  $n \rightarrow 1$ . The first of these cases,  $n \rightarrow 0$ , corresponds to the gyrotron mechanism. Referring to Eq. (24), the efficiency of the oscillator is proportional to the quantity

$$D_{\mu R} R_Q = -2 \frac{\beta_{\perp 0}}{\beta_{\perp 0}^2} \left( \frac{\sin \mu_R}{\mu_R} \right)^2 + \frac{1}{2} \frac{\omega_R L}{c} \frac{d}{d\mu_R} \left( \frac{\sin \mu_R}{\mu_R} \right)^2 . \quad (25)$$

The first term in the above expression is always negative, and its stabilizing effects are reduced if the ratio  $\beta_{\perp 0}^2/\beta_{\parallel 0}^2$  is large. If this ratio is large enough for this term to be omitted, a positive energy conversion can be obtained if the derivative  $dR_Q/d\mu_R$  is positive. This occurs in a number of intervals in the domain of  $\mu_R$ , the most prominent of which is  $-\pi < \mu_R < 0$ , and the maximum of  $dR_Q/d\mu_R = 0.54$  is attained at  $\mu_R = -1.3$ . Such negative values for  $\mu_R$  correspond to  $\omega_R > \Omega_0/\gamma_0$ , hence the wave frequency must exceed the relativistic electron gyrofrequency.

Let us now turn our attention to the interaction with luminous waves,  $n \rightarrow 1$ . In this case, the efficiency of the resonator, referring to Eq. (24), is proportional to

$$D_{\mu R} R_Q = \left[ 1 - 2 \frac{\beta_{\perp 0} (1 - \beta_{\parallel 0})}{\beta_{\perp 0}^2} \right] \left( \frac{\sin \mu_R}{\mu_R} \right)^2 + \mu_R \frac{d}{d\mu_R} \left( \frac{\sin \mu_R}{\mu_R} \right)^2 . \quad (26)$$

This function is plotted in Fig. (2) for  $\beta_{\parallel 0} = 0.1$  and (a)  $\beta_{\perp 0} = 0.7$ , (b)  $\beta_{\perp 0} = 0.425$ , and (c)  $\beta_{\perp 0} = 0.35$ . A number of interesting features can be observed in Eq. (26). First it is noted that  $D_{\mu R} R_Q$  (i.e.,  $n_{\ell}$ ) is an even function of  $\mu_R$ , therefore, contrary to the gyrotron mechanism, the interaction with luminous waves does not depend on the sign of the frequency mismatch,  $\Delta\omega_0 = \omega_R - \Omega_0/\gamma_0 - kv_{\parallel 0} = -2\mu_R v_{\parallel 0}/L$ . Instability occurs if either of two conditions are satisfied. The first is

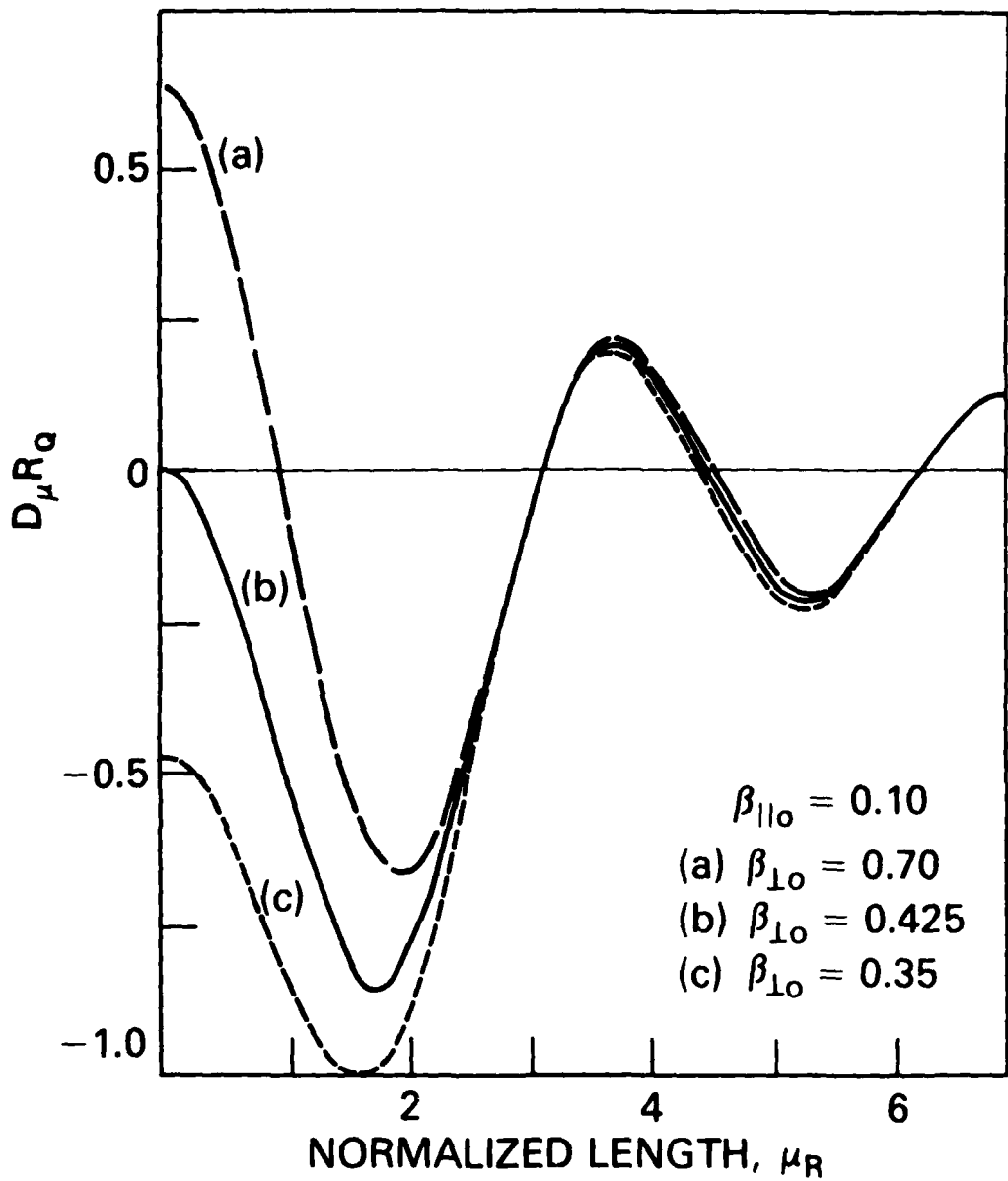


Fig. 2 — The function  $D_\mu R_Q(\mu_R)$ , which is proportional to the linear efficiency, versus  $\mu_R$ , which is proportional to the resonator length, for  $n=1$ ,  $\beta_{\parallel 0} = 0.1$  and (a)  $\beta_{\perp 0} = 0.70$ , (b)  $\beta_{\perp 0} = 0.425$ , and (c)  $\beta_{\perp 0} = 0.35$ .

$$\beta_{\perp 0}^2 > 2\beta_{\parallel 0} (1 - \beta_{\parallel 0}) , \quad (27)$$

and  $\mu_R = 0$ . If Eq. (27) is satisfied, the first term in Eq. (26) is positive, while the second term vanishes. Thus, contrary to the gyrotron mechanism, a positive efficiency can occur for  $\Delta\omega = 0$ , provided that Eq. (27) is satisfied. If Eq. (27) is well satisfied, the first term dominates up to the point  $|\mu_R| = 1.166$ , where  $\tan\mu_R = 2\mu_R$  and therefore  $-\mu_R dR_Q/d\mu_R = R_Q$ . Additional regions of instability occur when the second term is positive, provided that Eq. (27) is not too strongly violated. These regions cover the intervals  $j\pi < |\mu_R| < a_j - 1/a_j$ , where  $a_j = (2j+1)\pi/2$ ,  $j=1,2,3,\dots$ , and the upper limit is a good approximation to the solution of  $\tan\mu_R = \mu_R$ . In these regions,  $\mu_R dR_Q/d\mu_R$  reaches the maximum values  $1/(1+b_j)$  at  $|\mu_R| = b_j - 1/(\sqrt{2}b_j)$ , where  $b_j = (4j+1)\pi/4$ , and  $j$  is a positive integer.

### III. NONLINEAR THEORY

The linear analysis established that the cyclotron interaction with plane waves results in instability, even for luminous waves,  $n \rightarrow 1$ . In this section the nonlinear equations of motion are obtained, both on the fast and slow spatial scales. These equations are investigated and constants of the motion are obtained. The application of these invariants permits the analytical study of the conditions for energy depletion, the trajectories in phase space and the exact scaling relations for the efficiency. A single first-order differential equation is found to be sufficient to describe the evolution of the particles.

The nonlinear equations of motion are studied under the action of a uniform axial magnetic field,  $B_0 = B_0 \hat{e}_z$ , specified by its nonrelativistic electron gyrofrequency,  $\Omega_0 = eB_0/mc$ , and a steady state wave, whose vector potential is

$$A = A_0 \left[ \hat{e}_x \sin(kz - wt + \phi_0) + \epsilon \hat{e}_y \cos(kz - wt + \phi_0) \right]. \quad (28)$$

Only the forward wave is included in Eq. (28). Adding to Eq. (28) a similar expression, with  $k \rightarrow -k$  and  $\phi_0 \rightarrow \phi_0 + \pi$ , recovers Eq. (2). However, the backward wave has been omitted, since resonance with the forward component is assumed.

Although the natural independent variable for particle motion is time, it is convenient for oscillator configurations to adopt a Lagrangian representation, expressing the equations of motion in terms of the axial distance  $z$ . Since  $dt = dz/v_z$ , the phase of the wave as a function of  $z$  is given by

$$\psi(z) = k \int_0^z \left(1 - \frac{1}{n\beta_z(z')} \right) dz' + \psi_0 \quad (29)$$

where  $\beta_z = v_z/c$ . The equations of motion become

$$\begin{aligned} \frac{d}{dz} (\gamma\beta_x) &= A_0 \cos\psi \frac{d\psi}{dz} - \frac{\Omega_0}{c} \frac{\beta_y}{\beta_z}, \\ \frac{d}{dz} (\gamma\beta_y) &= -\epsilon A_0 \sin\psi \frac{d\psi}{dz} + \frac{\Omega_0}{c} \frac{\beta_x}{\beta_z}, \\ \frac{d}{dz} (\gamma\beta_z) &= -k A_0 \left( \frac{\beta_x}{\beta_z} \cos\psi - \epsilon \frac{\beta_y}{\beta_z} \sin\psi \right), \\ \frac{d}{dz} \gamma &= -k \frac{A_0}{n} \left( \frac{\beta_x}{\beta_z} \cos\psi - \epsilon \frac{\beta_y}{\beta_z} \sin\psi \right), \\ \frac{d}{dz} x &= \frac{\beta_x}{\beta_z}, \quad \frac{d}{dz} y = \frac{\beta_y}{\beta_x}, \end{aligned} \quad (30)$$

where  $A_0 = eA_0/mc^2$ ,  $\beta_x = v_x/c$ ,  $\beta_y = v_y/c$  and  $\gamma^2 = (1 - \beta_x^2 - \beta_y^2 - \beta_z^2)^{-1}$ .

Note that the first four of Eq. (30) are interrelated by the definition of  $\gamma$ . In addition, the equations for  $x$  and  $y$  can be integrated, in conjunction with the equations for  $\gamma\beta_y$  and  $\gamma\beta_x$ , respectively, to yield the constants of the motion

$$I_x = \gamma\beta_x - A_0 \sin\psi + \frac{\Omega_0}{c} y,$$

$$I_y = \gamma\beta_y - \epsilon A_0 \cos\psi - \frac{\Omega_0}{c} x.$$

These integrals can be used to assess the assumption of transverse uniformity implied by Eq. (28).

An additional invariant can be obtained from Eq. (30) by noting the equations for  $\gamma\beta_z$  and  $\gamma$ . This invariant<sup>30</sup> is

$$I_1 = \gamma(n - \beta_z) , \quad (31)$$

and its invariance is associated with the plane wave nature of the fields. When  $n=0$ , this invariant describes the conservation of axial momentum in the cut-off frame of the gyrotron.<sup>12</sup> If  $n > 1$ ,  $I_1$  is proportional to the conserved particle energy in the wave frame.<sup>33,34</sup> The significance of this invariant is that it indicates the possibility of complete energy depletion,  $\gamma=1$ , if the initial particle properties are such that  $I_1 = n$ . Denoting these initial properties with a subscript zero, the necessary condition for complete energy depletion is

$$\gamma_0 = \frac{n}{n-\beta_{z0}} . \quad (32)$$

Introducing the definition of  $\gamma_0$ , Eq. (32) can be written as

$$\beta_{z0}^2 = 2 \frac{\beta_{z0}}{n} \left( 1 - \beta_{z0} \frac{n^2+1}{2n} \right) , \quad (33)$$

where  $\beta_{z0}^2 = \beta_{x0}^2 + \beta_{y0}^2$ . An interesting observation is that when  $n=1$ , Eq. (33) reproduces the condition for the vanishing of the first term in the linear dispersion relation (see Eq. (26)). It should be noted that Eq. (32) or (33) represents only a necessary condition for complete energy depletion. The sufficient condition depends on whether the state of complete energy depletion is accessible by the particles. We will return to this point later.

The introduction of the invariants reduces the system of Eq. (30) formally to two coupled integro-differential equations for  $\gamma\beta_x$  and  $\gamma\beta_y$ . Following the usual procedure, we define

$$\beta_x = \beta_{\perp} \sin(\psi + \chi) , \quad (34)$$

$$\beta_y = \beta_{\perp} \cos(\psi + \chi) ,$$

where  $\beta_{\perp}$ ,  $\psi$  and  $\chi$  are functions of  $z$  varying slowly over a cyclotron period. Substituting Eq. (34) into Eq. (30) results in trigonometric functions with arguments  $\chi$  and  $2\psi + \chi$ . The  $2\psi + \chi$  terms phase-mix in a few wavelengths, hence the slow spatial scale equations are

$$\begin{aligned} \frac{d}{dz} (\gamma\beta_{\perp}) &= \frac{1+\epsilon}{2} k \left(1 - \frac{1}{n\beta_z}\right) A_0 \sin\chi , \\ \frac{d}{dz} (\gamma\beta_z) &= -\frac{1+\epsilon}{2} k \frac{\beta_{\perp}}{\beta_z} A_0 \sin\chi , \quad (35) \\ \frac{d}{dz} \chi &= -k \left[1 - \frac{1}{n\beta_z} \left(1 - \frac{\Omega_0}{\omega\gamma}\right)\right] + \frac{1+\epsilon}{2} k \frac{1}{\gamma\beta_{\perp}} \left(1 - \frac{1}{n\beta_z}\right) A_0 \cos\chi , \\ \frac{d}{dz} \gamma &= -\frac{1+\epsilon}{2} k \frac{\beta_{\perp}}{n\beta_z} A_0 \sin\chi . \end{aligned}$$

The above equations are interrelated by the definition of  $\gamma$  and the invariance of  $I_1$ . In addition, Eq. (35) possesses an additional invariant, given by

$$I_2 = (\gamma\beta_{\perp})^2 - (\gamma\beta_{\perp}) (1+\epsilon) A_0 \cos\chi - 2 \frac{\Omega_0}{kc} n\gamma . \quad (36)$$

It can be seen that when  $n=0$ ,  $\epsilon=0$  and  $\beta_z \rightarrow 0$ , the combination  $I_2 + I_1^2 + 1 + (\Omega_0/\omega)^2$  gives the corresponding gyrotron type invariant in the cut-off frame.<sup>12</sup> Also, when  $n > 1$ , then  $I_2$  transforms in the wave frame to the corresponding second invariant.<sup>33,34</sup> Furthermore, using the fast length scale Eq. (30), the derivative of  $I_2$  is

$$\frac{dI_2}{dz} = - (1-\epsilon) kA_0 \left\{ \left[ 1 - \frac{1}{n\beta_z} \left( 1 - \frac{\Omega_0}{\omega\gamma} \right) \right] \gamma\beta_\perp \sin(2\psi + \chi) + \left( 1 - \frac{1}{n\beta_z} \right) \frac{1+\epsilon}{2} A_0 \sin 2\psi \right\} . \quad (37)$$

Hence  $I_2$  is invariant also on the fast length scale, provided  $\epsilon=1$ .

The determination of the two invariants,  $I_1$  and  $I_2$ , allows us to study the trajectories in phase space. The appropriate coordinates for the two-dimensional representation are  $\chi$  and  $\gamma$ . Using the definition of  $\gamma$  and the invariance of  $I_1$  and  $I_2$  to eliminate  $\beta_z$  and  $\beta_\perp$  in terms of  $\gamma$  and  $\chi$  (and the initial conditions, denoted by subscript zero), we find that

$$\cos\chi = \frac{(1-n^2)(\gamma-\gamma_0)^2 + 2(\Delta\omega_0/\omega)\gamma_0(\gamma-\gamma_0) + (1+\epsilon)A_0\gamma_0\beta_{10}\cos\chi_0}{(1+\epsilon)A_0[(1-n^2)(\gamma-\gamma_0)^2 + 2(1-n\beta_{z0})\gamma_0(\gamma-\gamma_0) + (\gamma_0\beta_{10})^2]}^{1/2}, \quad (38)$$

where  $\Delta\omega_0 = \omega - \Omega_0/\gamma_0 - kv_{z0}$ .

We are primarily interested in the case of luminous waves,  $n=1$ . In this case, Eq. (38) takes on a rather simple form. The resultant equation is

$$qc_w - q^{1/2}\cos\chi = \text{const} , \quad (39)$$

where  $C_w$  is a constant proportional to the ratio of the initial frequency mismatch and the wave amplitude,

$$C_w = \frac{\gamma_0 \beta_{\perp 0}}{1 - \beta_{z0}} \frac{\omega - kv_{z0} - \Omega_0/\gamma_0}{\omega(1+\epsilon)A_0} , \quad (40)$$

and  $q$  is a linear function of  $\gamma$ ,

$$q = 2 \frac{1 - \beta_{z0}}{\gamma_0 \beta_{\perp 0}^2} (\gamma - \gamma_0) + 1. \quad (41)$$

It can be seen that  $q=1$  corresponds to the initial condition,  $\gamma=\gamma_0$ , hence the constant in Eq. (39) is equal to  $C_w - \cos x_0$ . In addition, depletion of the perpendicular or of the parallel energy, correspond to  $q=0$  and  $q=C_d$  respectively, where

$$C_d = 1 - \frac{2\beta_{z0}(1 - \beta_{z0})}{\beta_{\perp 0}^2} , \quad (42)$$

is a constant characterizing the anisotropy of the distribution. When  $C_d=0$ , complete depletion of the energy is possible, see Eq. (33).

For a positive frequency mismatch, that is, when  $C_w > 0$ , the phase space trajectories, obtained from Eq. (39), are shown schematically in Fig. (3). The arrows indicate the direction of particle motion. Both open and closed trajectories are possible in principle. The separatrix between these two families of curves is shown by the broken bell-shaped curve, described by the equation  $qC_w^2 - \cos^2 x = 0$  and defined only in the interval  $|x| \leq \pi/2$ . The largest value of  $q$  on the separatrix is at  $x=0$ ,  $q=C_w^{-2}$ . The vortex, or 0-point, of the closed trajectories is at  $x=0$ ,  $q = (2C_w)^{-2}$ .

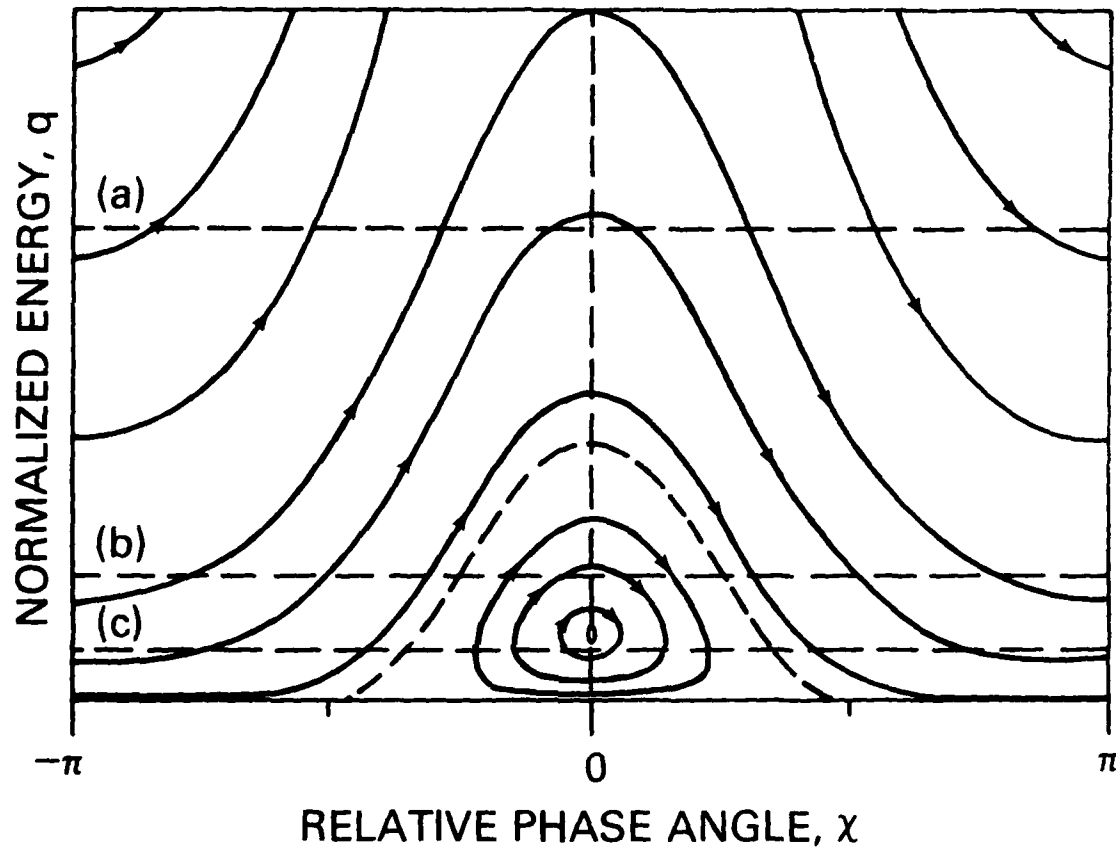


Fig. 3 — Trajectories in phase space coordinates  $q, \chi$ . The dashed curve is the separatrix. The dashed straight lines give the initial values,  $q=1$ , for (a)  $C_w > 1$ , (b)  $0.5 < C_w < 1$ , and (c)  $0 < C_w < 0.5$ .

For the curves in Fig. (3) to represent actual electron trajectories, they must intersect the initial condition line,  $q_0=1$ . The location of this line can be obtained in relation to the value of  $C_w$ . If  $C_w > 1$ , then the peak of the separatrix lies below the line  $q_0=1$  (line (a)), and all particles are untrapped. Trapped particles exist if  $C_w < 1$ , but always more than half of the initial phase angles  $x_0$  correspond to untrapped particles. Lines (b) and (c) in Fig. (3) describe the initial conditions,  $q_0=1$ , if  $0.5 < C_w < 1$  and  $0 < C_w < 0.5$ , that is, above and below the vortex, respectively.

When  $C_w < 0$ , the phase space trajectories are obtained from those in Fig. (3) by a reflection about the line  $x=\pi/2$ . The trajectories for  $C_w > 0$  and  $C_w < 0$  are shown in Figs. 4(a) and (b). Because of this symmetry, any particle, trapped or untrapped, in Fig. 4(a) has a corresponding particle in Fig. 4(b), which executes identical changes in  $q$  (or  $\gamma$ ). This recovers and extends to the nonlinear regime the linear result that the evolution is independent of the sign of the frequency mismatch (or  $C_w$ ). The phase plot in Fig. 4(c) corresponds to exact synchronism,  $C_w=0$ . In this case the separatrix reduces to the lines  $x=\pi/2$  and  $x=-\pi/2$  and all particles are semi-trapped. In this case the relative phase  $x$  is bounded, while the energy, or  $q$ , is bounded only from below. Whether the initial evolution in this case corresponds to net particle energy loss or gain depends on whether  $C_d > 0$  or  $C_d < 0$ , as has been shown in linear theory. However, it is clear from Fig. 4(c) that eventually all particles, regardless of their initial phase, will gain energy and will be tightly bunched in  $x$  (but not in energy), about  $x=-\pi/2$ . Accordingly, this configuration can be the basis for a particle

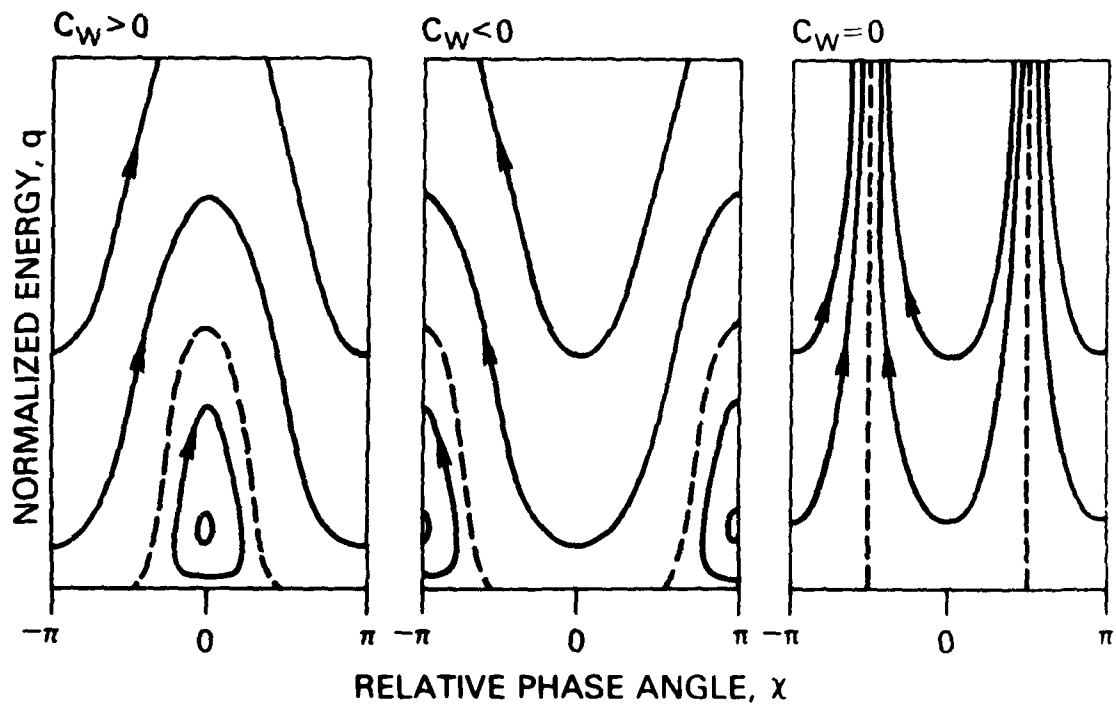


Fig. 4 — Comparison of phase space trajectories when (a)  $C_w > 0$ , (b)  $C_w < 0$ , and (c)  $C_w = 0$ .

accelerator. The details of such an application are currently under study and will be discussed in a separate publication.

The determination of the two invariants,  $I_1$  and  $I_2$ , which connect the three independent momentum components, makes possible the description of the electron evolution in terms of only one quantity, say  $q$  (i.e., the energy). When the index of refraction is unity, i.e.,  $n=1$ , the corresponding differential equation is

$$\frac{dq}{d\zeta} = - \operatorname{sgn}(\sin\chi) \frac{\left[ q - (qc_w - c_w + \cos\chi_0)^2 \right]^{\frac{1}{2}}}{q - c_d} \quad (43)$$

where  $\operatorname{sgn}$  is the sign function and the reduced length  $\zeta$  is defined as

$$\zeta = \frac{2(1+\epsilon)A}{\gamma_0 \beta_{\perp 0}} \left( \frac{1-\beta_{\perp 0}}{\beta_{\perp 0}} \right)^2 k(z-z_0) . \quad (44)$$

It can be seen that Eq. (43) is immediately integrable. The inversion of the resulting expression is straightforward only when  $c_w=0$ ,  $c_d < 0$ . This case is, however, uninteresting, since it corresponds to energy gain by the electrons.

In spite of the difficulties associated with the inversion of the integral of Eq. (43), useful information can still be obtained. It is noted that the solution of Eq. (43) has the form

$$q = q(\zeta_{\max}; \chi_0, c_w, c_d) , \quad (45)$$

where  $\zeta_{\max}$  is the value of  $\zeta$  corresponding to the length  $L$  of the interaction region in Eq. (44). In our Lagrangian representation, the efficiency is given by  $\eta = -\langle \gamma - \gamma_0 \rangle / (\gamma_0 - 1)$ , hence

$$\eta(\zeta_{\max}, C_w, C_d, C_n) = C_n (1-\langle q \rangle), \quad (46)$$

where the angular brackets denote an ensemble average over  $x_0$  and the coefficient  $C_n$  is defined by

$$C_n = \frac{\gamma_0 \beta_{z0}^2}{2(\gamma_0 - 1)(1 - \beta_{z0})} . \quad (47)$$

The efficiency, therefore, does not depend on the seven parameters  $k, A, \epsilon, L, \beta_{z0}, \beta_{z0}, \Omega_0$  arbitrarily but only on  $\zeta_{\max}, C_w, C_d$  and  $C_n$ . Further simplifications arise by the fact that  $C_n$  is just a multiplier of the efficiency expression. Large values of  $C_n$  are possible for a wide range of beam properties, as can be seen in Fig. (5). In this figure contour plots,  $C_n = \text{const}$ , are presented. In addition, Fig. (6) presents contour plots of  $C_d = \text{const}$ .

Before proceeding with the presentation of the results for the non-linear efficiency, it is worthwhile to rewrite the linear efficiency, Eq. (24), in terms of the variables defined above. We use the definitions of  $C_d, C_w, C_n$  and note from the definition of  $\zeta$  that it is related to  $\mu_0$  by  $C_w \zeta_{\max} = -2(1-C_d)\mu_0$ , where  $\mu_0$  is defined in Eq. (18) in terms of the initial values. Then from Eq. (24) the expression for the linear efficiency is obtained,

$$\eta_L = \frac{C_n}{C_w^2 (1-C_d)} \mu_0^2 (C_d + \mu_0 \frac{d}{d\mu_0}) \left( \frac{\sin \mu_0}{\mu_0} \right)^2 . \quad (48)$$

This expression has all the features expected from Eq. (46), since it involves a dependence on  $\zeta_{\max}$  (through  $\mu_0$ ), as well as  $C_w, C_d$  and  $C_n$ .

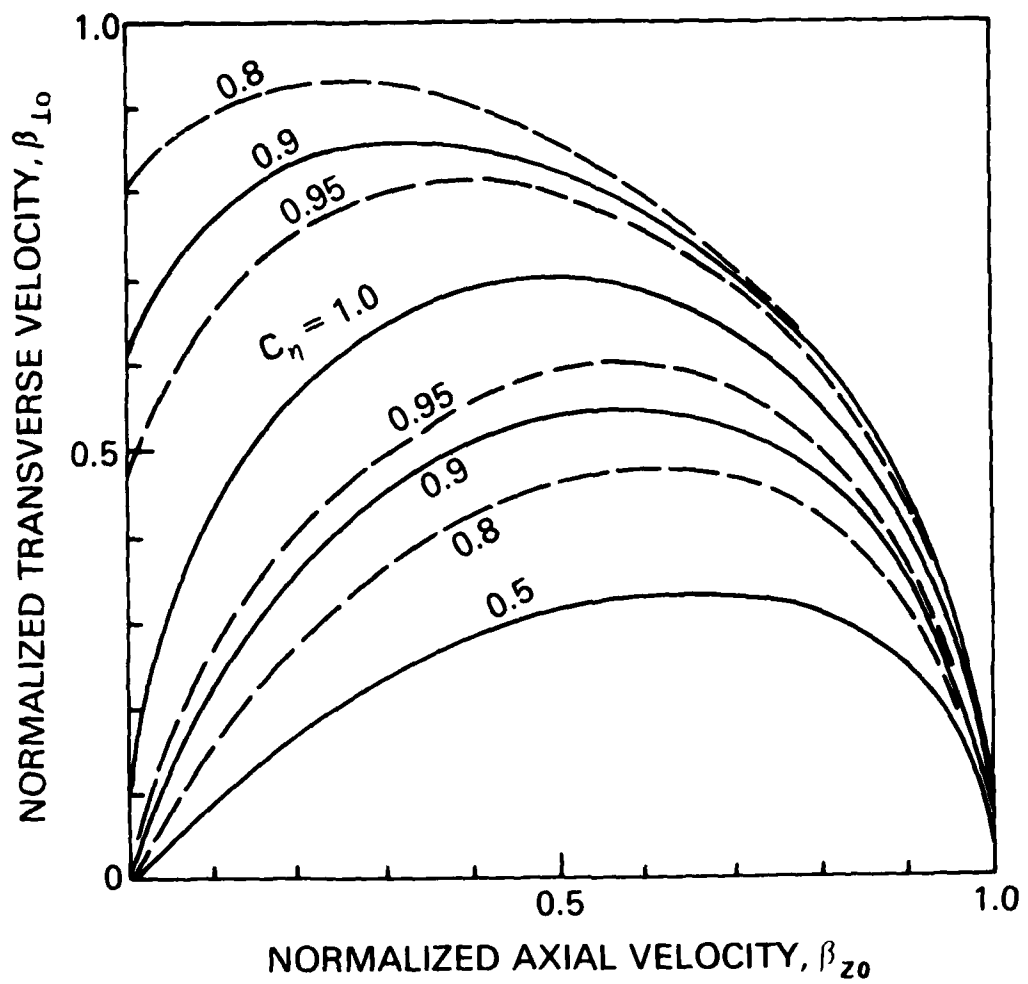


Fig. 5 — Contour plots for the efficiency coefficient  $C_\eta$  vs.  $\beta_{z0}$   $\beta_{z0}$ , the normalized transverse and axial electron velocities.

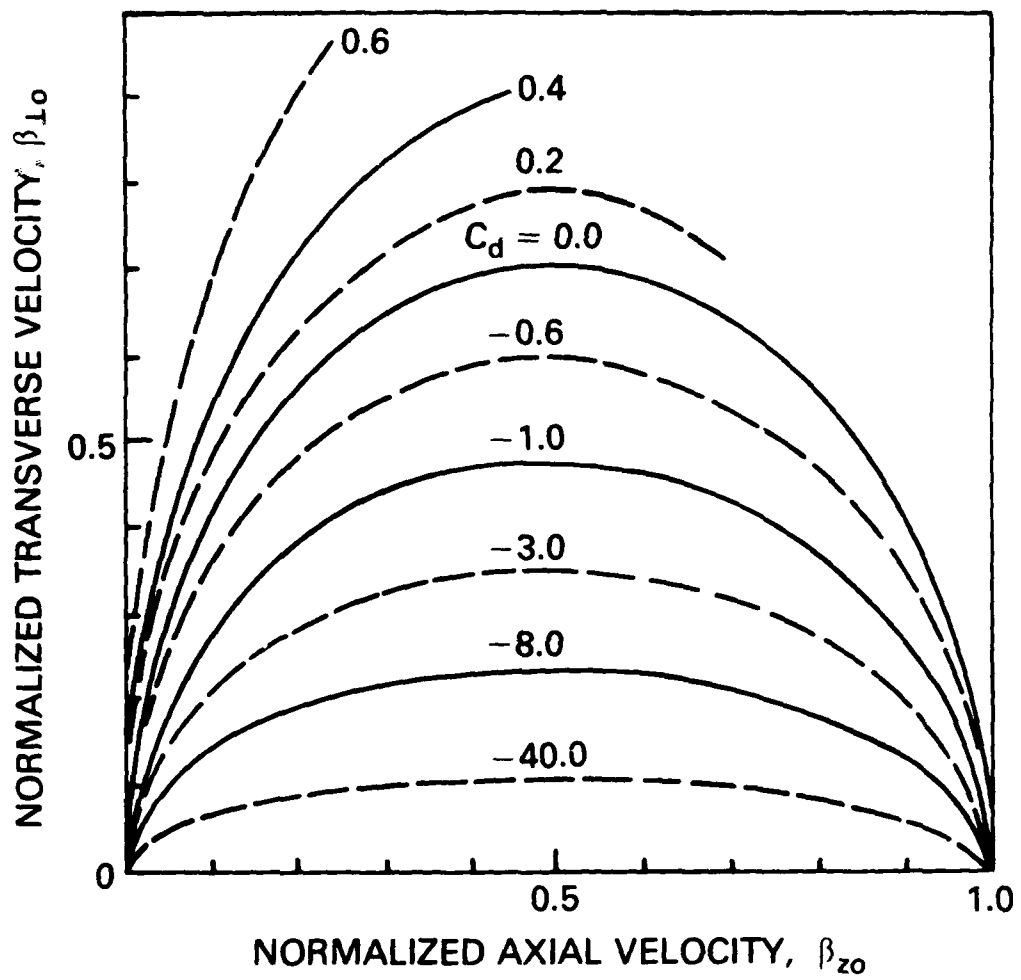


Fig. 6 — Contour plots for the anisotropy constant  $C_d$  vs.  $\beta_{zo}$  and  $\beta_{\perp o}$ .

Let us proceed now to solve for the nonlinear efficiency. Two numerical approaches are available, the first approach based on a numerical integration of the complete set of Eq. (30) to obtain the Lagrangian particle trajectories. The second approach requires the integration of Eq. (43) only. Both approaches have been used. In all cases, the agreement has been excellent. Equally excellent has been the agreement of the results with linear theory, when a sufficiently small amplitude or short interaction length has been employed in the simulations.

The dependence of the normalized efficiency  $n/C_n = 1 - \langle q \rangle$  on the reduced distance  $\mu_0$  is given by the solid curve in Fig. (7) for a distribution characterized by  $C_d = -2.5$  and a wave characterized by  $C_w = 1.4$ . Comparing this curve with linear theory has shown that initially, up to  $\mu_0 \approx 1.6$ , the evolution is essentially linear. Beyond that point, the efficiency undergoes oscillations in  $\mu_0$ , reminiscent of the corresponding linear behavior, except that these nonlinear oscillations do not diverge, while the linear result of Eq. (48) predicted divergent oscillations. The location of the relative maxima of the efficiency vs.  $\mu_0$  is however, in strikingly good agreement with linear theory. The first maximum is at  $\mu_0 = 3.7$ , and the corresponding optimized nonlinear efficiency is  $n/C_n = 0.164$ , approximately one half of the linear value  $n_\ell/C_n = 0.300$ . For these parameters, subsequent maxima correspond to negative values for the efficiency. The dashed curve corresponds to the values  $C_d = -2.5$  and  $C_w = 2.7$ . This case will be discussed later.

The contour plots of Fig. (8) show the normalized nonlinear efficiency,  $1 - \langle q \rangle$ , at the first maximum (the one near  $\mu_0 \approx 3.7$ ), for various values of the parameters  $C_d$  and  $C_w$ . As can be seen from the figure, large normalized efficiencies, e.g.,  $1 - \langle q \rangle \approx 0.15$ , are possible

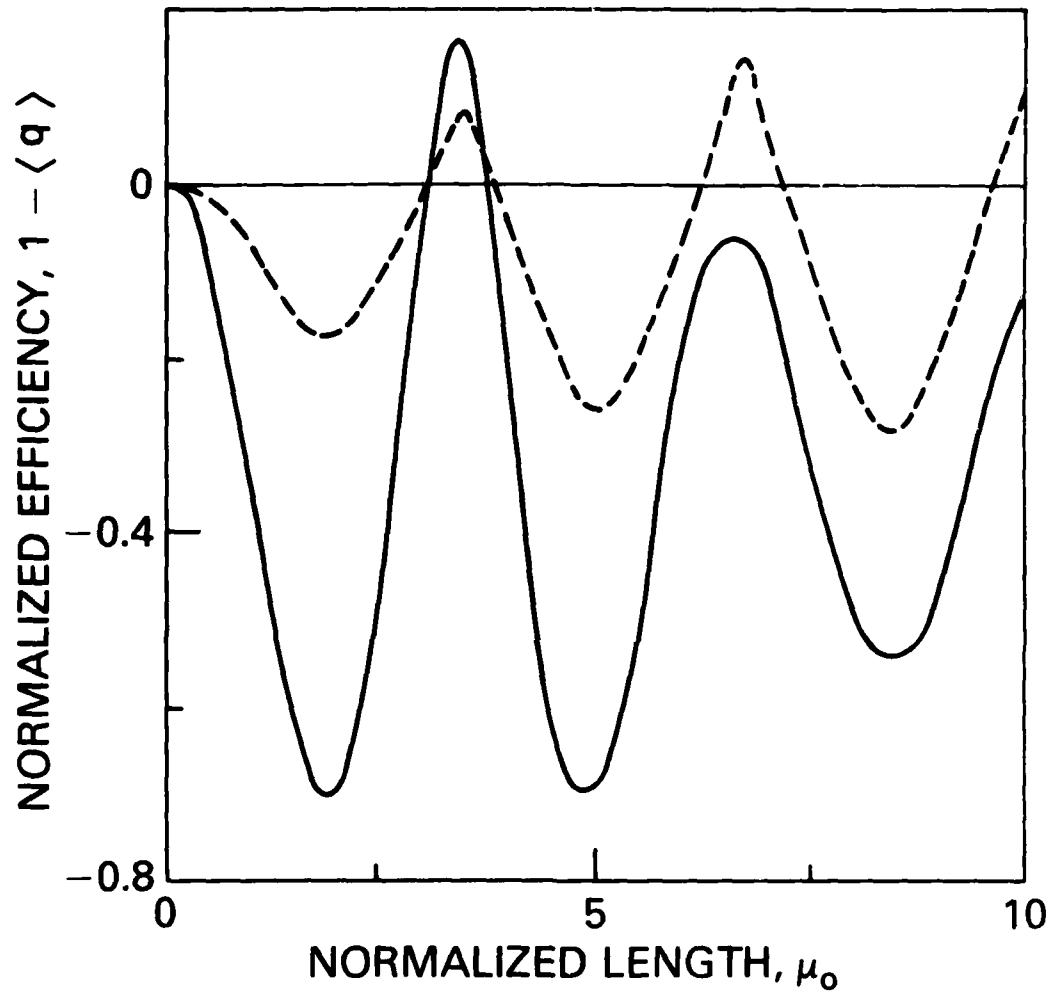


Fig. 7 — Spatial evolution of the normalized efficiency  $1 - \langle q \rangle = \eta/C_\eta$  for  $C_d = -2.5$  and  $C_w = 1.4$  (solid curve), as well as for  $C_d = -2.5$  and  $C_w = 2.7$  (dashed curve).

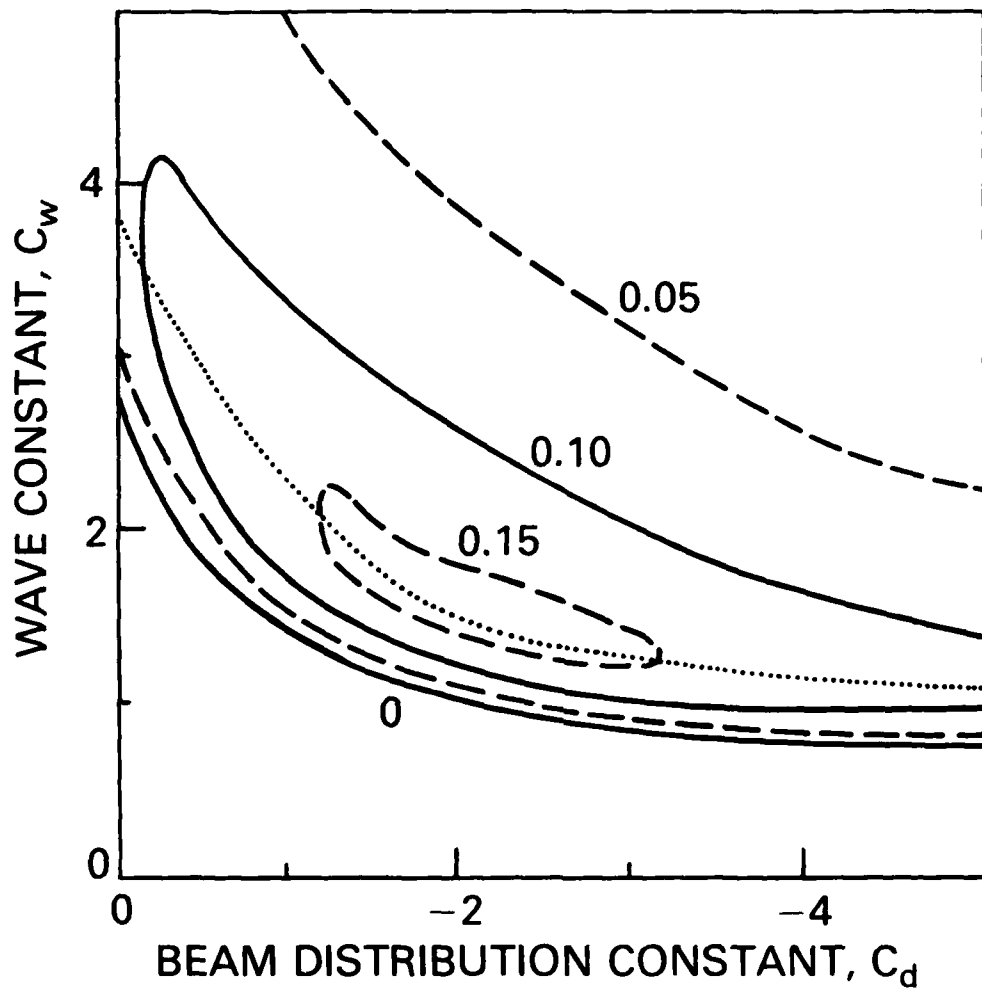


Fig. 8 — Contour plots of the normalized efficiency  $1-\langle q \rangle$  vs. the parameters  $C_d$  and  $C_w$  for an interaction length corresponding to the first efficiency maximum ( $\mu_0 \approx 3.7$ ). The dotted curve gives the value of  $C_w$  for maximum efficiency at any value of  $C_d$ .

over a wide range of beam distributions and ratios of frequency mismatch to radiation field amplitude. In addition, the dotted line in Fig. (8) gives the value of  $C_w$  required for optimal operation at a given value of  $C_d$ . For such values of  $C_w$ , the normalized efficiency as a function of  $C_d$  is given in Fig. (9). The overall maximum,  $1 - \langle q \rangle = 0.165$ , is obtained for  $C_d = -2.2$ ,  $C_w = 1.5$ .

The results presented so far apply to the first maximum of the nonlinear efficiency, at a point near  $\mu_0 = 3.7$ . This is not meant to imply that the first efficiency maximum is always dominant. For example, referring again to Fig. (7), it can be seen that increasing the value of  $C_w$ , causes the amplitude of the first efficiency maximum to decrease, and that of subsequent maxima to increase. When the point  $C_w = 2.7$  is reached (dashed curve), for which  $1 - \langle q \rangle$  maximizes near  $\mu_0 = 6.8$ , the normalized nonlinear efficiency is equal to  $1 - \langle q \rangle = 0.143$ . For even higher values of  $C_w$ , it is the third, fourth, etc. efficiency maximum that dominates. The same behavior is observed if  $-C_d$  is increased, keeping  $C_w$  constant. Contour plots for the efficiency at the second and subsequent maxima are very similar to those of Fig. (8), except that the curves are shifted to slightly higher values of  $C_w$  and  $-C_d$ .

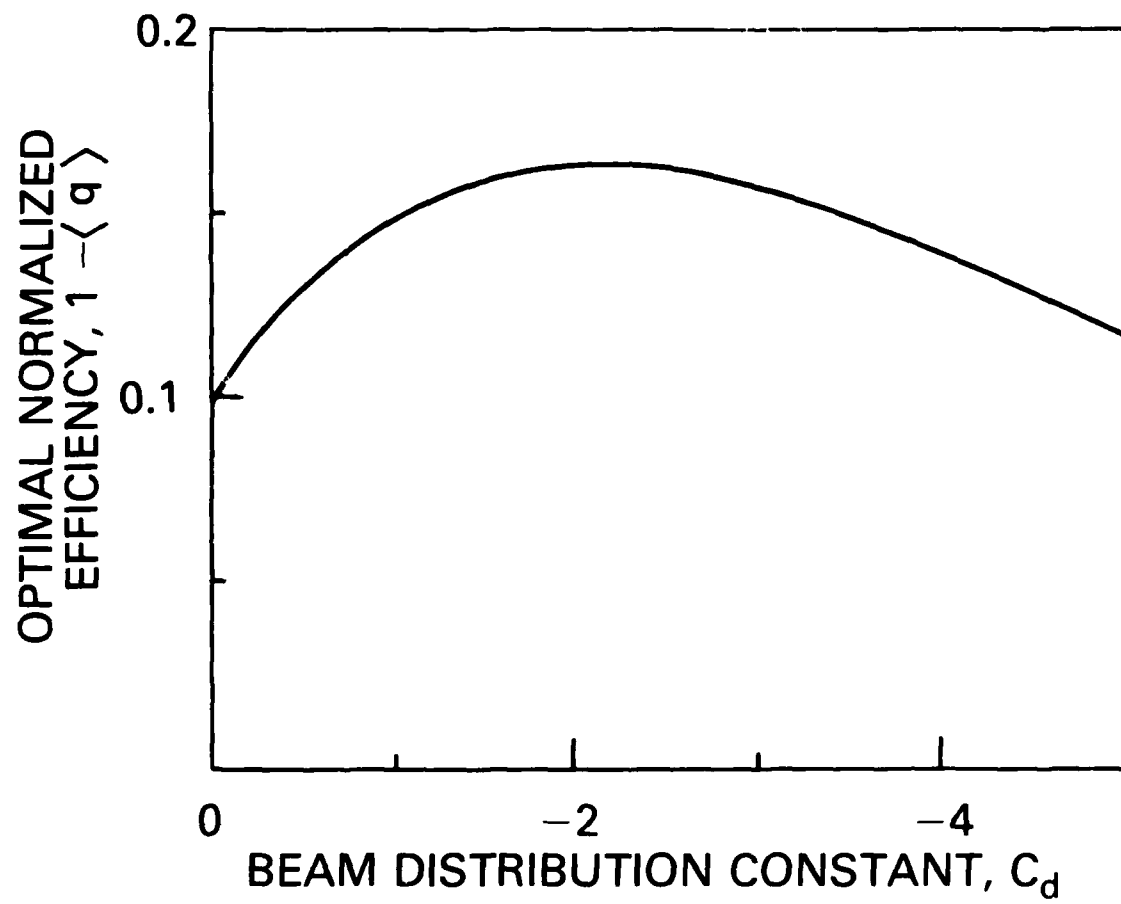


Fig. 9 — Optimal normalized efficiency (i.e., along the dotted curve of Fig. (8)), vs.  $C_d$ .

#### IV. DISCUSSION

In the previous two Sections, we have considered the linear and nonlinear electron cyclotron interaction with (primarily) luminous waves. From that analysis, results have been obtained regarding the stability of these waves and the nonlinear steady-state performance. In this Section, we conclude with various aspects concerning the practical feasibility of a device based on this analysis. We show that this interaction has weak temperature requirements ( $\delta\beta_{z0}/\beta_{z0} \ll 1$ ) and that excellent mode selection can be achieved. One example of a cyclotron maser is given and the use of this interaction as a free-electron laser is discussed. Finally, the possibility of improving the nonlinear efficiency (up to  $n \approx 0.60$ ) is discussed.

##### (a) Temperature requirements.

Let us consider first the effects associated with a thermal spread,  $\delta\beta_{z0}$  and  $\delta\gamma_0$ , of the beam electrons. The sharpness of the resonance in both linear and nonlinear theory is characterized by the parameter  $\mu_0$ , which can be written as

$$\mu_0 = \pi \frac{L}{\lambda} \left[ 1 + \frac{\Omega/\gamma_0 - \omega}{kc\beta_{z0}} \right] , \quad (49)$$

where  $\lambda = 2\pi/k$  is the radiation wavelength. From the dependence of the efficiency on  $\mu_0$ , it is seen that  $|\delta\mu_0| \ll \pi/4$  is required. With regard to the parallel velocity, this translates to the requirement

$$\frac{\delta\beta_{z0}}{\beta_{z0}} \ll \frac{1}{4} \frac{\lambda}{L} \frac{kc\beta_{z0}}{|\Omega/\gamma_0 - \omega|} . \quad (50)$$

For conventional cyclotron maser operation,  $\omega \gtrsim \Omega/\gamma_0 + kc\beta_{z0}$  and this requirement gives  $\delta\beta_{z0}/\beta_{z0} \ll \lambda/4L$ , prohibiting<sup>15</sup> operation in a system longer than a few wavelengths. However, when  $\omega = kc$ , the symmetry about  $\mu_0 = 0$  allows a choice of operating point with  $\omega < \Omega/\gamma_0 + kc\beta_{z0}$ . In particular, if the wave is suppressed (e.g., by a polygonal ray-path in a multi-mirror resonator) and the choice is made that

$$\mu_0 = \pi \left( \frac{L}{\lambda} + \frac{1}{4} \right) , \quad (51)$$

where a local maximum of the efficiency is located, the requirement is simply

$$\frac{\delta\beta_{z0}}{\beta_{z0}} \ll 1. \quad (52)$$

For the same operation, the requirement for  $\delta\gamma_0$  is

$$\frac{\delta\gamma_0}{\gamma_0} \ll \frac{1}{4} \beta_{z0} \frac{\lambda}{L} , \quad (53)$$

which may be more restrictive.

As regards the other significant parameters of the interaction, the requirement  $|\delta C_d| \ll 1 - C_d$  gives a condition supplementary to Eq. (53),

$$\frac{\delta\gamma_0}{\gamma_0} \ll (\gamma_0 \beta_{z0})^2 , \quad (54)$$

while the condition on the parallel velocity is less restrictive than (52). Similarly, the condition  $|\delta C_w| \ll C_w$  is satisfied if the above conditions are satisfied, except that in the highly relativistic limit,  $\beta_{z0} \rightarrow 1$ , an additional condition is imposed, viz.

$$\frac{\delta\beta_{z0}}{\beta_{z0}} \ll \frac{1-\beta_{z0}}{1-C_d} . \quad (55)$$

(b) Mode Selectivity.

Transverse and longitudinal mode selectivity can be dealt separately. We will not deal in any detail with the former. It is expected that by an appropriate design of the mirrors, only the lowest order transverse mode will be intercepted, while the higher order modes will suffer from diffraction losses.

As far as the longitudinal modes are concerned, we first seek to determine the number of modes that fill the positive gain curve segment, at whose peak the desired longitudinal mode is located. Since the half-width of the gain curve is  $|\delta\mu| \lesssim \pi/4$ , it can be seen from Eq. (49) that the number  $\delta l$  of longitudinal mode pairs (in addition to the mode at which operation is desired) within the positive gain segment is

$$\delta l \lesssim \frac{\beta_{z0}}{2(1-\beta_{z0})} . \quad (56)$$

Thus, no competing axial modes are present if  $\beta_{z0} < 2/3$ . On the other hand, many modes will be excited in the case of a highly relativistic electron beam with  $\beta_{z0} \rightarrow 1$ .

An additional point to be considered is whether the operation of the device at a certain efficiency maximum is accompanied by the presence of a different longitudinal mode which might correspond to a value of  $\mu_0$  lying within a different positive segment of the gain curve. This question is particularly important when there are many wavelengths within the resonator. In that case, the operation is seen from Eq. (51) to

require a large value of  $\mu_0$  and the broken line in Fig. (7) indicates that more than one gain segment corresponds to positive gain. Such undesired modes can be suppressed by the introduction of distributed feedback. Inherent means for mode selection are also available. Thus, it can be seen from Eq. (49) that if the choice

$$\beta_{z0} = \frac{1}{2j + 1} \quad (57)$$

is made, where  $j$  is an integer, then the closest potentially unstable mode falls at the next  $(2j+1)$ -th maximum of the gain curve. If  $j$  is not too small, then it is expected that this maximum may correspond to negative gain, thus guaranteeing the absence of any competing modes.

(c) Example of cyclotron maser operation.

Before proceeding, it is necessary to present a numerical example, in order to demonstrate how our results can be applied to a particular design. We consider an interaction at the third maximum of the gain curve. As can be seen from Eq. (51), temperature effects are reduced by choosing a system length equal to  $3\lambda$ . The normalized efficiency at the third maximum is  $\eta/C_n = -0.156$ , for  $C_d = -2.9$ ,  $C_w = \pm 3.0$  and  $\mu_0 = \pm 10.1$ . A value  $\beta_{z0} = 0.143 (=1/7)$  guarantees the absence of any competing modes (see Eq. (57)) and Eq. (53) gives the condition  $\delta\gamma_0/\gamma_0 \ll 1.2\%$ . From the definition of  $C_d$ , Eq. (42) (or, from Fig. (6)), it can be found that  $\beta_{10} = 0.25$ , hence  $\gamma_0 = 1.0433$  corresponding to a beam energy of 22.2 keV. Then from the definition of  $C_n$ , Eq. (47), or, from Fig. (5), it is found that  $C_n = 0.88$ . Therefore, the nonlinear efficiency is  $\eta = 0.137$ . For the above values and the definition of  $C_w$  (Eq. (40)), the normalized vector potential of the

radiation field, assuming linear polarization, has the value  $A_0 = 1.55 \times 10^{-2}$ . The external magnetic field gives a gyrofrequency satisfying  $\Omega_0/\omega = 1.055$  and the frequency mismatch is  $\Delta\omega_0/\omega = (\omega - \Omega_0/\gamma_0 - kv_{\perp 0})/\omega = -0.154$ . Finally, by choosing a wavelength  $\lambda = 2$  mm, this example requires an external magnetic field of  $B_0 = 56.5$  kG for a radiation field amplitude of  $E_0 = 833$  sV/cm ( $\approx 250$  kV/cm) and frequency  $\omega = 0.942 \times 10^{12}$  sec $^{-1}$  ( $= 150$  GHz). For an incident beam current of 20 A, the radiated power is 61 kW.

(d) Free-electron-laser type operation.

An interesting variant to the study presented here is the possibility of using the interaction for the excitation of waves with a frequency shifted significantly above the gyrofrequency.<sup>35</sup> It can be seen from the definition of  $C_w$  that the frequency is given by

$$\omega = \frac{\Omega_{z0}}{\gamma_0(1-\beta_{z0})} + C_w \frac{1+\epsilon}{\gamma_0 \beta_{\perp 0}} \frac{eE_0}{mc} , \quad (58)$$

where  $E_0 = \omega A_0/c$  is the amplitude of the electric component of the radiation field. The operating frequency is essentially given by the first term in Eq. (58). Defining the axial relativistic factor,  $\gamma_{z0} = (1-\beta_{z0}^2)^{-1/2}$ , the operating frequency is accurately given by

$$\omega = (1 + \beta_{z0}) \gamma_{z0}^2 \frac{\Omega_0}{\gamma_0} \quad (59)$$

and bears the same form as the free-electron laser frequency,<sup>36,37</sup> employing a magnetic wiggler.

Since the relativistic gyrofrequency depends on the mass factor  $\gamma_0$ , the actual quantity that multiplies the nonrelativistic gyrofrequency to give the operating frequency is  $I_1^{-1}$ , where  $I_1 = \gamma_0(1-\beta_{z0})$  is the first invariant. For high operating frequencies, it is required that  $I_1^{-1} \gg 1$ . This requirement, together with the desire that  $C_\eta$  be not too much less than unity (in order to achieve adequate efficiencies) requires that  $-C_d \ll 1$ . Thus, as can be seen from Fig. (9), efficiencies of the order of 10% are to be expected. For example,  $\omega/\Omega_0 = 10$  requires  $I_1 = 0.1$ . Taking  $\gamma_0 = 50$ , gives  $\beta_{z0} = 0.998$  and  $\beta_{\perp 0} = 0.06$ . Then  $C_d = -0.11$ , giving  $n/C_\eta = 0.102$ , and  $C_\eta = 0.917$ , and the result is an efficiency  $\eta = 9.36\%$ . (Of course, higher efficiencies can be obtained by adopting efficiency enhancement schemes, as discussed in IV(e) below.) In this example, it is required that  $C_w = 3.6$  and  $\mu_0 = 3.6$ . Choosing a wavelength of  $\lambda=0.2$  mm ( $f = 1.5$  THz) and a system length  $L = 1m = 5000 \lambda$ , it is found that an external magnetic field of strength  $B_0 = 47.5$  kGs is needed. Furthermore, assuming a beam current of 10 A, the radiated power is equal to  $P_{rad} = 23.4$  MW.

(e) Efficiency enhancement.

The nonlinear analysis of Sec. III shows that the performance of an oscillator operating with luminous waves is limited to efficiencies  $\eta \lesssim 16\%$ . Here we will outline briefly a scheme which can improve the performance of the interaction dramatically. We introduce a two-stage oscillator configuration, in which the first stage (the prebuncher) acts to pre-bunch the particles in their relative angle  $x$ , without significantly changing particle momentum. The second stage (the converter) converts the kinetic energy of the bunch to radiation energy. A 100% conversion

is possible, if the bunch is perfect and  $C_d = 0$ .

In the prebuncher we require a combination of a "large" frequency mismatch and "small" radiation field amplitude, such that  $|C_{w1}| \gg 1$ . In this stage the electrons are highly untrapped and only negligible energy exchange occurs. To first order  $x$  is

$$x^{(1)} = x_0 + \left( C_{w1} - \frac{\cos x_0}{2} \right) \zeta \quad (60)$$

where  $C_d = 0$  has been assumed. For  $x_0$  uniformly distributed in the interval  $(0, 2\pi)$ , Eq. (60) describes the formation of a bunch.

The extraction of particle energy occurs in the converter. From the discussion of Sec. III (see also Fig. (3)), it is recalled that a particle on the separatrix eventually loses all its kinetic energy, if  $C_d = 0$ , as is assumed here. Since the bunch has a spread in  $x$  rather than in  $q$ , it is necessary to arrange the converter parameters so that  $C_{w2} = 1$ . With an appropriate choice of  $C_{w1}$ , the bunch will be centered at the peak of the separatrix. The center of the bunch will thus be able to convert all its energy to radiation energy, by choosing the appropriate length for the converter section. Examining the bunch coherence from Eq. (60) it can be estimated that efficiencies of the order of 60% are attainable.

As an example of a two-stage oscillator we consider the case  $C_{w1} = 7.5$ ,  $C_d = 0$ , with a discontinuity in the radiation field amplitude,  $C_{w2} = 1.0$ , for  $\zeta > \zeta_1$ . The evolution of the efficiency for this case is shown in Fig. (10). The oscillatory curve gives the evolution when the first oscillator is sufficiently long,  $\zeta_1 \rightarrow \infty$ . However, if the location of the discontinuity is appropriately chosen, the ensuing evolution is

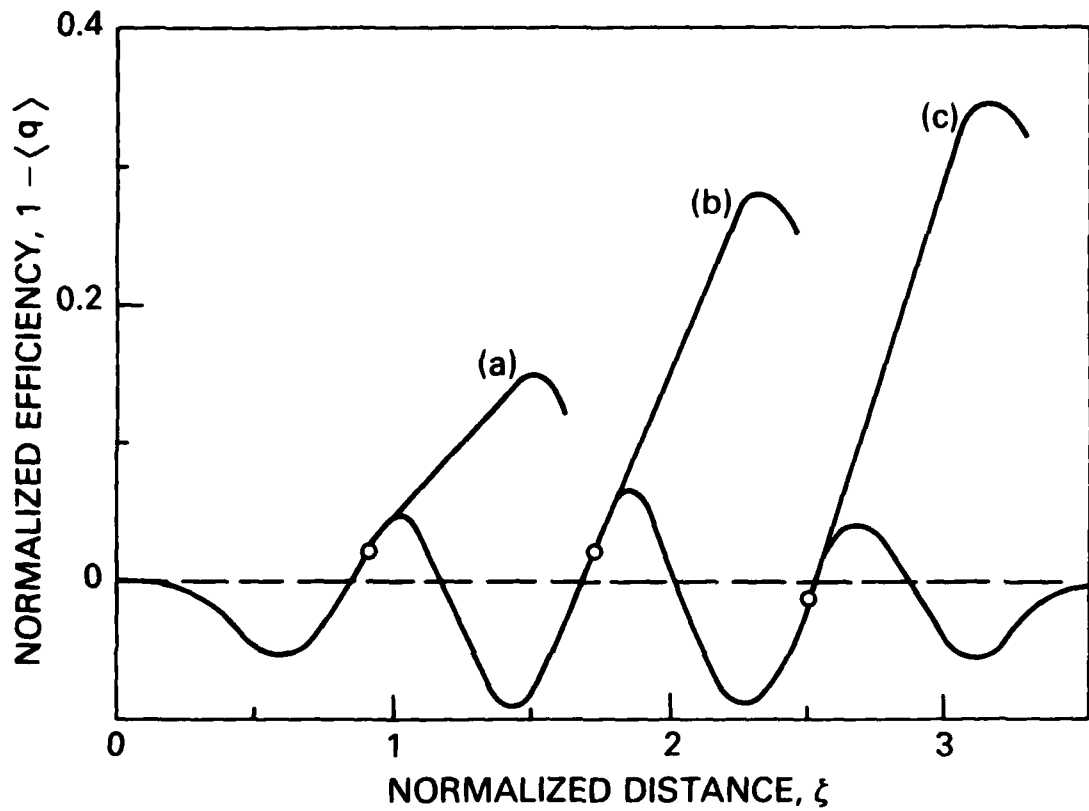


Fig. 10 — Efficiency enhancement in a two-stage oscillator configuration. The oscillatory curve gives the nonlinear normalized efficiency vs. normalized distance for  $C_{w1} = 7.5$  and  $C_d = 0$  in a single resonator. The introduction of a second resonator with  $C_{w2} = 1.0$  at  $\xi = \xi_1$ , shown by the small circles, improves the overall efficiency. The cases shown correspond to (a)  $\xi_1 = 0.90$ , (b)  $\xi_1 = 1.72$ , and (c)  $\xi_1 = 2.50$ .

characterized by substantially increased efficiency. Thus, for the choices  $\zeta_1 = 0.90, 1.72$ , and  $2.50$ , shown in the figure by the small circles, the evolution of the efficiency in the second oscillator, where  $C_{w2} = 1.0$ , is shown by the curves (a), (b), and (c). This procedure yields the optimal values of the efficiency  $\eta = 0.15, 0.28$ , and  $0.35$  at the positions  $\zeta_2 = 1.5, 2.3$ , and  $3.1$ , respectively. This clearly demonstrates the principle of efficiency enhancement in a two-stage oscillator.

#### ACKNOWLEDGMENTS

This work has been supported by the Office of Naval Research and the U. S. Department of Energy. Discussions with W. M. Manheimer have been very useful.

## REFERENCES

1. R. Q. Twiss, Australian J. Phys. 11, 564 (1958).
2. A. V. Gaponov, Izv. VUZ. Radiofizika, 2, 450 (1959).
3. R. H. Pantell, Proc. IRE, 47, 1146(1959).
4. J. L. Hirschfield, I. B. Bernstein, and J. M. Wachtel, IEEE J. Quantum Electron., QE-1, 237(1965).
5. A. V. Gaponov, M. I. Petelin, and V. K. Yulpatov, Radiophys. Quantum Electron., 10, 794 (1967).
6. M. Borenstein and W. E. Lamb, Jr., Phys. Rev., A5, 1298 (1972).
7. Edward Ott and Wallace M. Manheimer, IEEE Trans. PS-3, 1 (1975).
8. P. Sprangle and Wallace M. Manheimer, Phys. Fluids 18, 224 (1975).
9. V. L. Granatstein, P. Sprangle, M. Herndon and R. K. Parker, J. Applied Phys. 46, 2021 (1975).
10. V. A. Flyagin, A. V. Gaponov, M. I. Petelin, and V. K. Yulpatov, IEEE Trans. MTT-25, 514 (1977).
11. J. L. Hirshfield and V. L. Granatstein, IEEE Trans. MTT-25, 522 (1977).
12. P. Sprangle and A. T. Drobot, IEEE Trans. MTT-25, 528 (1977).
13. W. M. Manheimer and V. L. Granatstein, NRL Memorandum Report 3493 (1977).
14. A. A. Andronov, V. A. Flyagin, A. V. Gaponov, A. L. Gol'denberg, M. I. Petelin, V. G. Usov, and V. K. Yulpatov, Infrared Physics 18, 385 (1978).
15. H. Jory, S. Hegji, J. Shiverly and R. Symons, Microwave J. 21, 30 (1978).
16. K. R. Chu, Phys. Fluids 21, 2354 (1978).
17. J. L. Seftor, V. L. Granatstein, K. R. Chu, P. Sprangle and M. E. Read, IEEE J. Quantum Electron., QE-15, 849 (1979).
18. M. E. Read, R. M. Gilgenbach, R. Lucey, Jr., K. R. Chu, A. T. Drobot and V. L. Granatstein, IEEE Trans. MTT (in press).

19. D. V. Kisell', G. S. Korablev, V. G. Navel'yev, M. I. Petelin, and Sh. Ye. Tsimring, Radio Engineering and Electronics Physics 19, 95 (1974).
20. Yu. V. Bykov and A. L. Gol'denberg, Radiophys. Quantum Electron. 18, 791 (1975).
21. P. Sprangle and Robert A. Smith, NRL Memorandum Report 3983 (1979).
22. K. R. Chu, M. E. Read, and A. K. Ganguly, NRL Memorandum Report 4051 (1979).
23. M. E. Read, K. R. Chu, and A. J. Dudas, NRL Memo Rpt. 4169 (1980).
24. M. A. Moiseev, G. S. Nusinovich, Radiophys. Quantum Electron. 17, 1305 (1974).
25. G. S. Nusinovich, Radiophys. Quantum Electron. 19, 1301 (1976).
26. I. G. Zarnitsyna and G. S. Nusinovich, Radiophys. Quantum Electron. 20, 313 (1977).
27. J. L. Vomvoridis and P. Sprangle, NRL Memorandum Report 4426 (1980).
28. D. J. Dialetis and K. R. Chu, NRL Memorandum Report
29. The case of the electron beam propagating across the resonator axis is considered in P. Sprangle, W. M. Manheimer and J. L. Vomvoridis, NRL Memorandum Report 4366(1980); also submitted to Phys. Rev. A.
30. The backward wave can be suppressed by a multi-mirror resonator arrangement, in which the radiation follows a polygonal path. Also, the effects of the backward wave are negligible when  $\Delta\omega \ll k_V$ .
31. K. R. Chu and J. L. Hirshfield, Phys. Fluids 21, 461 (1978).
32. S. K. Ride and W. B. Colson, Appl. Phys. 20, 41 (1979).
33. C. S. Roberts and S. J. Buchsbaum, Phys. Rev. 135, A381 (1964).
34. R. F. Lutomirski and R. N. Sudan, Phys. Rev. 147, 156 (1966).
35. J. L. Hirshfield, K. R. Chu and S. Kainer, Appl. Phys. Lett. 33, 847 (1978).
36. P. Sprangle and R. A. Smith, Phys. Rev. A21, 293 (1980).
37. P. Sprangle, Cha-Mei Tang and W. M. Manheimer, Phys. Rev. A21, 302 (1980).

DISTRIBUTION LIST\*

Naval Research Laboratory  
4555 Overlook Avenue, S.W.  
Washington, D.C. 20375

Attn: Code 1000 - CAPT E. E. Henifin  
1001 - Dr. A. Berman  
4700 - Dr. T. Coffey (25 copies)  
4701 - Mr. J. Brown  
4740 - Dr. V. L. Granatstein (20 copies)  
4740 - Dr. K. R. Chu  
4740 - Dr. C. W. Roberson  
4740 - Dr. M. E. Read  
4790 - Dr. P. Sprangle (100 copies)  
4790 - Dr. M. Lampe  
4790 - Dr. W. M. Manheimer  
6603S - Dr. W. W. Zachary  
6650 - Dr. L. Cohen  
6656 - Dr. N. Seeman  
6805 - Dr. S. Y. Ahn  
6805 - Dr. A. Ganguly  
6805 - Dr. N. R. Vanderplaats  
6850 - Dr. L. R. Whicker  
6875 - Dr. R. Wagner

On Site Contractors:

Code 4740 - Dr. J. M. Baird (B-K Dynamics)  
4740 - Dr. L. Barnett (B-K Dynamics)  
4740 - Dr. D. Dialetis (SAI)  
4740 - Dr. Y. Y. Lau (SAI)  
4740 - Dr. J. S. Silverstein (HDL)  
4790 - Dr. A. T. Drobot (SAI)  
4790 - Dr. C. M. Tang (JAYCOR)  
4790 - Dr. J. Vomvoridis (JAYCOR) (50 copies)  
4790 - Dr. H. Freund (SAI)

\* Every name listed on distribution gets one copy except for those where extra copies are noted.

Dr. Tony Armstrong  
SAI, Inc.  
P. O. Box 2351  
La Jolla, CA 92038

Dr. Robert Behringer  
ONR  
1030 E. Green  
Pasadena, CA 91106

Dr. G. Bekefi (5 copies)  
Massachusetts Institute of Technology  
Bldg. 26  
Cambridge, MA 02139

Dr. Arden Bement (2 copies)  
Deputy Under Secretary of  
Defense for R&AT  
Room 3E114, The Pentagon  
Washington, D.C. 20301

Dr. T. Berlincourt  
Code 420  
Office of Naval Research  
Arlington, VA 22217

Dr. I. B. Bernstein (2 copies)  
Yale University  
Mason Laboratory  
400 Temple Street  
New Haven, CT 06520

Dr. Fred Burskirk  
Physics Department  
Naval Postgraduate School  
Monterey, CA 93940

Dr. K. J. Button  
Massachusetts Institute of Technology  
Francis Bitter National Magnet  
Laboratory  
Cambridge, MA 02139

Dr. Gregory Canavan  
Director, Office of Inertial Fusion  
U. S. Department of Energy  
M.S. C404  
Washington, D.C. 20545

Dr. C. D. Cantrell  
T-DOT, MS210  
Los Alamos Scientific Laboratory  
Los Alamos, NM 87545

Dr. Weng Chow  
Optical Sciences Center  
University of Arizona  
Tucson, AZ 85721

Dr. Peter Clark  
TRW, Building R-1, Room 1096  
One Space Park  
Redondo Beach, CA 90278

Dr. Robert Clark  
P. O. Box 1929  
Washington, D.C. 20013

Dr. William Colson  
Quantum Institute  
Univ. of California at Santa Barbara  
Santa Barbara, CA 93106

Dr. William Condell  
Code 421  
Office of Naval Research  
Arlington, VA 22217

Dr. Richard Cooper  
Los Alamos Scientific Laboratory  
P. O. Box 1663  
Los Alamos, NM 87545

Cmdr. Robert Cronin  
NFOIO Detachment, Suitland  
4301 Suitland Road  
Washington, D.C. 20390

Dr. R. Davidson (5 copies)  
Plasma Fusion Center  
Massachusetts Institute of Technology  
Cambridge, MA 02139

Dr. John Dawson (2 copies)  
Physics Department  
University of California  
Los Angeles, CA 90024

Defense Technical Information Center  
(12 copies)  
Cameron Station  
5010 Duke Street  
Alexandria, VA 22313

Dr. Francesco De Martini  
Instituto de Fisica  
"G. Marconi" Univ.  
Piazzo delle Science, 5  
ROMA00185 ITALY

Prof. P. Diamant  
Columbia University  
Dept. of Electrical Engineering  
New York, NY 10027

Prof. H. J. Doucet (5 copies)  
Ecole Polytechnique  
91128 Palaiseau  
Paris, France

Dr. John Elgin (2 copies)  
Imperial College  
Dept. of Physics (Optics)  
London SWF, England

Dr. David D. Elliott  
SRI International  
333 Ravenswood Avenue  
Menlo Park, CA 94025

Dr. Norval Fortson  
Department of Physics  
University of Washington  
Seattle, WA 98195

Director (2 copies)  
National Security Agency  
Fort Meade, MD 20755  
ATTN: Mr. Richard Foss, A42

Dr. Robert Fossum, Director  
(2 copies)  
DARPA  
1400 Wilson Boulevard  
Arlington, VA 22209

Dr. Edward A. Frieman  
Director, Office of Energy Research  
U. S. Department of Energy  
M.S. 6E084  
Washington, D.C. 20585

Dr. George Gamota (3 copies)  
OUSDRE (R&AT)  
Room 3D1067, The Pentagon  
Washington, D.C. 20301

Dr. Richard L. Garwin  
IBM, T. J. Watson Research Center  
P. O. Box 218  
Yorktown Heights, NY 10598

Dr. Edward T. Gerry, President  
W. J. Schafer Associates, Inc.  
1901 N. Fort Myer Drive  
Arlington, VA 22209

Dr. Avraham Gover  
Tel Aviv University  
Fac. of Engineering  
Tel Aviv, ISRAEL

Dr. A. H. Guenter  
Chief Scientist  
Air Force Weapons Laboratory  
Kirtland AFB, NM 87117

Mr. Donald L. Haas, Director  
DARPA/STO  
1400 Wilson Boulevard  
Arlington, VA 22209

Dr. P. Hammerling  
La Jolla Institute  
P. O. Box 1434  
La Jolla, CA 92038

Director  
National Security Agency  
Fort Meade, MD 20755  
ATTN: Mr. Thomas Handel, A2L3

Dr. William Happer  
560 Riverside Drive  
New York City, NY 10027

Dr. Tom Kupper  
Optical Sciences Center  
University of Arizona  
Tucson, AZ 85721

Dr. Robert J. Hermann  
Assistant Secretary of the  
Air Force (RD&L)  
Room 4E856, The Pentagon  
Washington, D.C. 20330

Dr. Willis Lamb  
Optical Sciences Center  
University of Arizona  
Tucson, AZ 85721

Dr. Rod Hiddleston  
KMS Fusion  
Ann Arbor, MI 48106

Mr. Mike Lavan  
BMDATC-O  
ATTN: ATC-O  
P. O. Box 1500  
Huntsville, AL 35807

Dr. J. L. Hirshfield (2 copies)  
Yale University  
Mason Laboratory  
400 Temple Street  
New Haven, CT 06520

Dr. John D. Lawson (2 copies)  
Rutherford High Energy Lab  
Chilton  
Didcot, Oxon OX11 0OX  
ENGLAND

Dr. R. Hofland  
Aerospace Corp.  
P. O. Box 92957  
Los Angeles, CA 90009

Mr. Ray Leadabrand  
SRI International  
333 Ravenswood Avenue  
Menlo Park, CA 94025

Dr. Benjamin Huberman  
Associate Director, OSTP  
Room 476, Old Executive Office Bldg.  
Washington, D.C. 20506

Mr. Barry Leven  
NISC/Code 20  
4301 Suitland Road  
Washington, D.C. 20390

Dr. S. F. Jacobs  
Optical Sciences Center  
University of Arizona  
Tucson, AZ 85721

Dr. Donald M. LeVine (3 copies)  
SRI International  
1611 N. Kent street  
Arlington, VA 22209

Dr. Howard Jory (3 copies)  
Varian Associates, Bldg. 1  
611 Hansen Way  
Palo Alto, CA 94303

Dr. Anthony T. Lin  
University of California  
Los Angeles, CA 90024

Mr. Eugene Kopf  
Principal Deputy Assistant  
Secretary of the Air Force (RD&L)  
Room 4E964, The Pentagon  
Washington, D.C. 20330

Director (2 copies)  
National Security Agency  
Fort Meade, MD 20755  
ATTN: Mr. Robert Madden, R/SA

Prof. N. M. Kroll  
La Jolla Institutes  
P. O. Box 1434  
La Jolla, CA 92038

Dr. Joseph Mangano  
DARPA  
1400 Wilson Boulevard  
Arlington, VA 22209

Dr. S. A. Mani  
W. J. Schafer Associates, Inc.  
10 Lakeside Office Park  
Wakefield, MA 01880

Dr. Mike Mann  
Hughes Aircraft Co.  
Laser Systems Div.  
Culver City, CA 90230

Dr. T. C. Marshall  
Applied Physics Department  
Columbia University  
New York, NY 10027

Mr. John Meson  
DARPA  
1400 Wilson Boulevard  
Arlington, VA 22209

Dr. Pierre Meystre  
Projektgruppe fur Laserforschung  
Max Planck Gesellschaft  
Garching, Munich GERMANY

Dr. Gerald T. Moore  
Optical Sciences Center  
University of Arizona  
Tucson, AZ 85721

Dr. Philip Morton  
Stanford Linear Accelerator Center  
P. O. Box 4349  
Stanford, CA 94305

Dr. Jesper Munch  
TRW  
One Space Park  
Redondo Beach, CA 90278

Dr. George Neil  
TRW  
One Space Park  
Redondo Beach, CA 90278

Dr. Kelvin Neil  
Lawrence Livermore Laboratory  
Code L-321, P. O. Box 808  
Livermore, CA 94550

Dr. Milton L. Noble (2 copies)  
General Electric Company  
G. E. Electronic Park  
Syracuse, NY 13201

Prof. E. Ott (2 copies)  
University of Maryland  
Dept. of Physics  
College Park, Md. 20742

Dr. Richard H. Pantell  
Stanford University  
Stanford, CA 94305

Dr. Richard M. Patrick  
AVCO Everett Research Lab., Inc.  
2385 Revere Beach Parkway  
Everett, MA 02149

The Honorable William Perry  
Under Secretary of Defense (R&E)  
Office of the Secretary of Defense  
Room 3E1006, The Pentagon  
Washington, D.C. 20301

Dr. Alan Pike  
DARPA/STO  
1400 Wilson Boulevard  
Arlington, VA 22209

Dr. Hersch Piloff  
Code 421  
Office of Naval Research  
Arlington, VA 22217

Dr. Charles Planner  
Rutherford High Energy Lab  
Chilton  
Didcot, Oxon, OX11 0OX,  
ENGLAND

Dr. Michal Poole  
Daresbury Nuclear Physics Lab.  
Daresbury, Warrington  
Cheshire WA4 4AD  
ENGLAND

Dr. Don Prosnitz  
Lawrence Livermore Laboratory  
Livermore, CA. 94550

**Dr. D. A. Reilly**  
AVCO Everett Research Lab.  
Everett, MA 02149

**Dr. James P. Reilly**  
W. J. Schafer Associates, Inc.  
10 Lakeside Office Park  
Wakefield, MA 01880

**Dr. A. Renieri**  
C.N.E.N.  
Div. Nuove Attività  
Dentro di Frascatti  
Frascatti, Rome  
ITALY

**Dr. Daniel N. Rogovin**  
SAI  
P. O. Box 2351  
La Jolla, CA 92038

**Dr. Michael Rosenbluh**  
MIT - Magnet Lab.  
Cambridge, MA 02139

**Dr. Marshall N. Rosenbluth**  
Institute for Advanced Study  
Princeton, NJ 08540

**Dr. Eugene Ruane (2 copies)**  
P. O. Box 1925  
Washington, D.C. 20013

**Dr. Antonio Sanchez**  
MIT/Lincoln Laboratory  
Room B231  
P. O. Box 73  
Lexington, MA 02173

**Prof. S. P. Schlesinger**  
Columbia University  
Dept. of Electrical Engineering  
New York, NY 10027

**Dr. Howard Schlossberg**  
AFOSR  
Bolling AFB  
Washington, D.C. 20332

**Dr. Starley Schneider**  
Rotodyne Corporation  
26628 Fond Du Lac Road  
Palos Verdes Peninsula, CA 90274

**Dr. Marlan O. Scully**  
Optical Sciences Center  
University of Arizona  
Tucson, AZ 85721

**Dr. Robert Sepucha**  
DARPA/STO  
1400 Wilson Boulevard  
Arlington, VA 22209

**Dr. A. M. Sessler**  
Lawrence Berkeley Laboratory  
University of California  
1 Cyclotron Road  
Berkeley, CA 94720

**Dr. Earl D. Shaw**  
Bell Labs  
600 Mountain Avenue  
Murray Hill, NJ 07974

**Dr. Chan-Ching Shih**  
R&D Associates  
P. O. Box 9695  
Marina del Rey, CA 92091

**Dr. Kenneth Smith**  
Physical Dynamics, Inc.  
P. O. Box 556  
La Jolla, CA 92038

**Mr. Todd Smith**  
Hansen Labs  
Stanford University  
Stanford, CA 94305

**Dr. Joel A. Snow**  
Senior Technical Advisor  
Office of Energy Research  
U. S. Department of Energy, M.S. E084  
Washington, D.C. 20585

**Mrs. Alma Spring**  
DARPA/Administration  
1400 Wilson Boulevard  
Arlington, VA 22209

SRI/MP Reports Area G037 (2 copies)  
333 Ravenswood Avenue  
Menlo Park, CA 94025  
ATTN: D. Leitner

Dr. Abraham Szoke  
Lawrence Livermore Laboratory  
MS L-470, P. O. Box 808  
Livermore, CA 94550

Dr. Milan Tekula  
AVCO Everett Research Lab.  
2385 Revere Beach Parkway  
Everett, MA 02149

Dr. R. Temkin (2 copies)  
Plasma Fusion Center  
Massachusetts Institute of Technology  
Cambridge, MA 02139

Dr. John E. Walsh  
Department of Physics  
Dartmouth College  
Hanover, NH 03755

Dr. Wasneski (2 copies)  
Naval Air Systems Command  
Department of the Navy  
Washington, D.C. 20350

Lt. Col. W. Whitaker  
Defense Advanced Research Projects  
Agency  
1400 Wilson Boulevard  
Arlington, VA 22209

Ms. Bettie Wilcox  
Lawrence Livermore Laboratory  
ATTN: Tech. Info. Dept. L-3  
P. O. Box 808  
Livermore, CA 94550

Dr. A. Yariv  
California Institute of Tech.  
Pasadena, CA 91125

